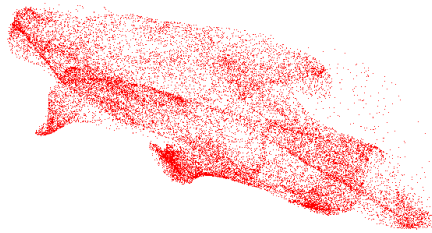


**Predicting induced chaos in the population dynamics of an
insect species**



Dimitrios Nerantzis

A thesis submitted in partial fulfilment of the requirements for the degree of Master of
Science of Imperial College London and Diploma of Imperial College London.

September 2011

Στον πατέρα μου Στέφανο,
στη μητέρα μου Αγγελική,
στην αδερφή μου Θεοδώρα και
στον παππού μου Δημήτριο.

Ο επιστήμονας δεν μελετάει τη φύση επειδή είναι χρήσιμη. Την μελετάει επειδή τον ενθουσιάζει και τον ενθουσιάζει επειδή είναι όμορφη. Αν η φύση δεν ήταν όμορφη, δεν θα άξιζε να τη γνωρίσουμε και αν δεν άξιζε να τη γνωρίσουμε, δε θα άξιζε και να τη ζήσουμε.

H. Poincaré

Abstract

A difference equation model based in biological mechanisms is presented describing the laboratory population dynamics of the flour beetle *Tribolium freemani*. This is the first time a model for this insect species is presented. The model was fitted to laboratory data and evaluated. The results suggest that the model's predictive ability is good and that the biological mechanisms taken under consideration are sufficient to explain the dynamics. For certain parameter manipulations the model predicts chaotic behaviour with strong statistical confidence. These manipulations can be experimentally imposed. An experiment is proposed in order to verify the model's predictions.

Contents

- 1. Introduction** 1
- 2. Experimental Data** 2
- 3. The mathematical model** 5
- 4. Methods**
 - Parameter Estimation 8
 - Model Evaluation 9
 - Confidence Intervals 10
 - Lyapunov Exponents 11
 - Software 12
- 5. Model Fitting Results**
 - Parameter Estimation 13
 - Model Evaluation 14
- 6. Chaos and Discrete State Dynamics**
 - Chaotic Dynamics 22
 - Discrete State Dynamics and Underlying chaos 27
 - A Proposed Experimental Scheme 30
- 7. Discussion** 35
- 8. Acknowledgements** 37
- 9. References** 38
- 10. Appendix**

Parameter Estimation	42
The Inhibition Function	43
Results from Statistical Tests on the Residuals	45
Time Series and Corresponding One-Step Predictions	47
Other Model Trials	49
Lyapunov Dimension	51

Introduction

Henri Poincare was the first man who realised how complicated the behaviour of a deterministic dynamical system can be while studying, what is known in celestial mechanics as, “The three body problem” [1]. It was Edward Lorenz though, who gave rise to the study of chaos with his discovery of a strange attractor in a meteorological model [2]. Today chaos, a term first given by Li and Yorke in [3] is well established and demonstrated in many scientific fields [4-7].

The main feature among the different mathematical definitions of chaos is the sensitivity to initials conditions [8]. Sensitivity to initial conditions means that even the smallest disturbance on a deterministic dynamical system will have an amplified effect over the course of time. This characteristic though, is not necessarily sufficient for a dynamical system to be chaotic.

Robert May popularized chaos among the ecologists, by revealing that simple deterministic population models can have a very complicated (chaotic) dynamical behaviour which in first sight might appear as random [9,10]. May’s hypothesis that the erratic fluctuations observed in population data could be explained by simple deterministic rules, started a new era in population dynamics. But the initial excitement has turned to scepticism [11]. Until today there are only a few cases providing enough evidence of chaos in ecological systems [12-17]. As mentioned in [16] this could be attributed to the difficulties incorporated in analyzing ecological data but it could also be the case that chaos is indeed rare in ecology. Searching for chaos in time series data is based in methods which try to reconstruct the attractor of the system [18] or to calculate Lyapunov exponents [19,20] for which a positive value is an indication of chaos. The main problems though, in using the above methods are the need for long term data and noise, which in ecological data is always present.

In [13,17] Costantino et al. followed a different path. Instead of analysing time series, they built a discrete time (difference equations) population model for the flour beetle *Tribolium castaneum* based on the cannibalistic relationships among different life stages of the species. They provided evidence from real data of the model’s predictions by

manipulating experimentally a number of parameters demonstrating transitions in the dynamical behaviour of the population from stable cycles to invariant loops and chaos. Besides providing evidence for the predicted chaos, the importance of their work was also the demonstration that a mathematical model in ecology can actually be very accurate and provide explanations for the mechanisms governing the dynamics of a species proving at the same time that ecology does not need to have mainly a descriptive character.

This project, following the work on the dynamics of the *T. castaneum* [13,17,21,22], presents a discrete time model, proposed by R. Costantino, for the population dynamics of *T. freemani*. The difference in this species, from *castaneum*, is that apart from cannibalism there is a tactile mechanism which causes a larva to delay its pupation when sensing crowding of larvae population [23-25]. The model was fitted to laboratory data and evaluated in data both used and unused in the fitting. The evaluation suggests that the model's predictions are accurate, indicating that the mechanisms of cannibalism and inhibition of pupation are sufficient to describe the dynamics of the species. For certain parameter values the model predicts, with strong statistical confidence, chaotic behaviour. A discrete state version of the model (system state variables take only integer values) is considered and a connection is made between the chaotic dynamics of the continuous state model and the corresponding dynamics of the discrete model. At last, an experimental scheme is outlined on how the model's prediction about the induced chaotic dynamics could be verified considering the presence of noise in real data.

Experimental Data

The data were obtained from an experiment done by Robert F. Costantino. The data consisted of twelve replicates, each of 80 weeks in length. All replicates were initiated from the same conditions (number of insects). The first three replicates were the control replicates for which the habitat volume (expressed in units of grams of medium) was kept stable at 54g. For the rest of the replicates the habitat volume, for each transition from time t to time $t+1$, was given randomly fluctuating values but for different "colour" (different kind of autocorrelation in the successive random volume values) of

fluctuations for replicates 4-6, 7-9 and 10-12. Replicates 3, 6, 9 and 12 were not used in the fitting in order to have the chance to evaluate the model using data not used for fitting. The different “colours” of noise were not intended for the purposes of this project, but there was no problem in using them for fitting the model. The numbers of ordinary larvae, delayed larvae, pupae and adults were counted every two weeks.

As an example, in figures 1a-1d the volume fluctuations are shown for the first replicate in each group of replicates (1-3, 4-6, 7-9 and 10-12). Again, the label of the y axes in each graph, “Volume in grams”, means that volumes were expressed in grams of medium.

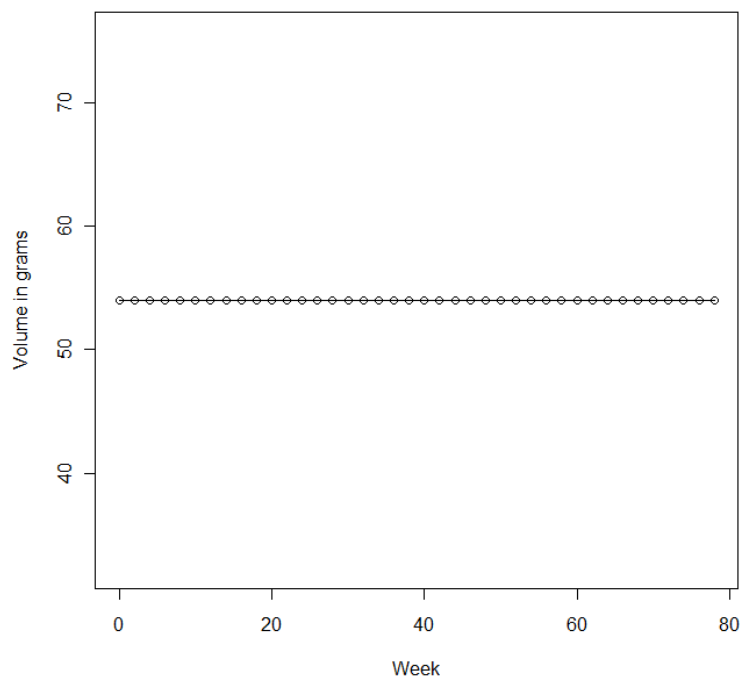


Figure 1a: Volumes in replicate 1. Constant at 54g.

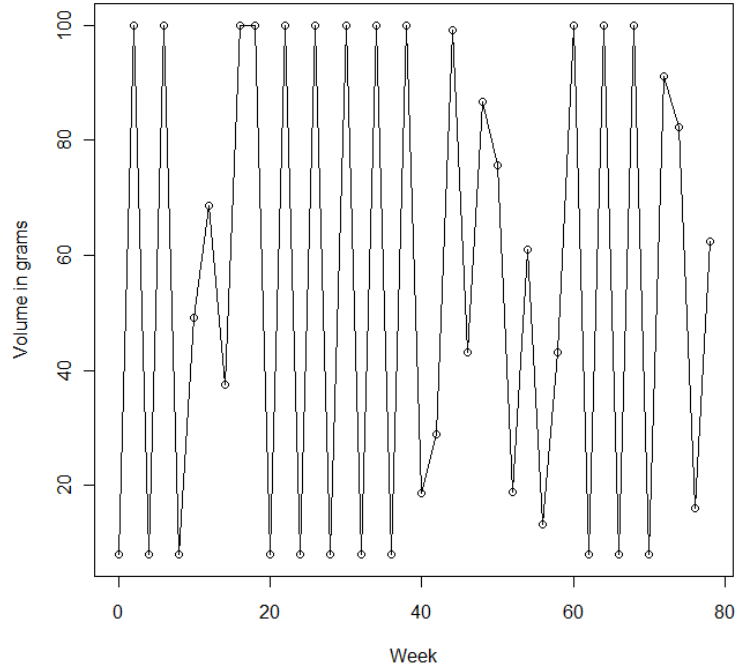


Figure 1d: Volumes in replicate 10. Blue noise, negative autocorrelation.

The mathematical model

The beetles belonging to the *Tribolium* genus have four life stages: egg, larva, pupa and adult [17]. Many species of the genus *Tribolium* are cannibalistic, larvae cannibalize on eggs while adults cannibalize on both eggs and pupae [17]. In previous work [13,17,21,22], it has been demonstrated that a discrete time model, built under the assumption that cannibalism is driving the population dynamics of *T. castaneum*, can predict with accuracy the observed, from laboratory data, dynamics. In *T. freemani*, which is the case of this work, there is another biological mechanism that plays a major role in the population dynamics of the species along with cannibalism. Crowding of larvae (10 larvae per gram of media) inhibits their pupation [23-25]. The following deterministic discrete time model was proposed by R. F. Costantino and it is based on the biological mechanisms sketched above.

$$\begin{aligned}
L_{t+1}^{(1)} &= bA_t \exp \left[\left(-c_{e1}L_t^{(1)} - c_{e2}L_t^{(2)} - c_{ea}A_t \right) / V_t \right] \\
L_{t+1}^{(2)} &= \left\{ (1 - \mu_1)L_t^{(1)} \left[1 - f \left(\frac{L_t^{(1)}}{V_t} \right) \right] + (1 - \mu_2)L_t^{(2)} \left[1 - f \left(\frac{L_t^{(2)}}{V_t} \right) \right] \right\} (1 - E) \\
P_{t+1} &= (1 - \mu_1)L_t^{(1)} f \left(\frac{L_t^{(1)}}{V_t} \right) + (1 - \mu_2)L_t^{(2)} f \left(\frac{L_t^{(2)}}{V_t} \right) \\
A_{t+1} &= P_t \exp \left(-c_{pa}A_t / V_t \right) + (1 - \mu_a)A_t
\end{aligned} \tag{1}$$

The state variable $L_t^{(1)}$ is the number of ordinary larvae, $L_t^{(2)}$ are the delayed (to go into pupation) larvae, P_t is the number of non-feeding larvae, pupae and callow adults and A_t are the sexually mature adults at time t . The time scale is 2 weeks which is approximately the time needed for an individual to go from larva to pupa (in the absence of crowding) and from pupa to adult under the experimental conditions. The eggs are not considered in the model since it takes 2-3 days for an egg to hatch and because eggs are difficult to count experimentally. Habitat size V_t is a time-dependent, external forcing parameter (random or periodic). The exponential terms in the model account for cannibalism, with $c_{e1}, c_{e2}, c_{ea}, c_{pa}$ being the coefficients of cannibalism of $L^{(1)}, L^{(2)}$ larvae on eggs, adults on eggs and adults on pupae respectively. For example the term $\exp(-c_{pa}A/V)$ in the last equation is the probability that a pupa in a habitat of volume V at time t will not get eaten by an adult until time $t+1$. The average adult fecundity is denoted as b while the mortality rates for $L^{(1)}, L^{(2)}$ and adults are denoted as μ_1, μ_2, μ_a . The parameter E is the experimentally imposed emigration rate of $L^{(2)}$ larvae (set at $E=0.55$ in the experiment). Emigration of $L^{(2)}$ would take place naturally in a population outside the lab.

The function $f\left(\frac{L_t^{(n)}}{V_t}\right) = \frac{1 + \exp(-h_1 h_2)}{1 - 2 \exp(-h_1 h_2) + \exp(-h_1 h_2 + h_2 L_t^{(n)} / V_t)}$ where $n=1, 2$ gives

the fraction of $L_t^{(n)}$ larvae that will be pupae at time $t+1$. The parameter h_1 is the density of larvae where the pupation rate is 50%, and h_2 is the “sharpness” of the “shoulder” of the f function (see appendix). Each larval stage ($L^{(1)}$ and $L^{(2)}$) influences the pupation of only larvae of the same stage.

What should be demanded from a deterministic model in biology is to describe mathematically the main biological mechanisms driving the dynamics of the system. But, every dynamical system in nature is subject to noise. In ecological systems noise (or else stochasticity) is distinguished in two types, demographic and environmental [21]. Demographic noise accounts for random (unpredicted by the deterministic model) variations in birth, mortality and migration rate of individuals which in turn they have an impact on the total population. Environmental noise accounts for the variation in vital rates caused by environmental changes which affect a large part or the whole population. For example a period of extreme low temperatures which might increase the mortality rate of a whole species population is environmental noise. Since the insect populations were cultured in a controlled laboratory environment it is reasonable to expect that the type of noise present in the data would be demographic.

In order to incorporate demographic noise into the deterministic noise we add “square-root” scale noise (see [17] for theory). This means that, under some prerequisites, a discrete time system of equations $X_{t+1} = f(X_t)$ where, $f : A \subseteq \mathfrak{R}^n \rightarrow A$, would take the form $X_{t+1} = \left[\sqrt{f(X_t)} + E_t \right]^2$ with $E_t = [E_{1t}, E_{2t}, \dots, E_{nt}]^T$ being a random vector having approximately normal distribution. Applying the above to the first three equations of the deterministic model we get the stochastic version,

$$\begin{aligned}
L_{t+1}^{(1)} &= (\sqrt{bA_t \exp[(-c_{e1}L_t^{(1)} - c_{e2}L_t^{(2)} - c_{ea}A_t)/V_t]} + E_{1t})^2 \\
L_{t+1}^{(2)} &= \left[\sqrt{\left\{ (1 - \mu_1)L_t^{(1)} \left[1 - f\left(\frac{L_t^{(1)}}{V_t}\right) \right] + (1 - \mu_2)L_t^{(2)} \left[1 - f\left(\frac{L_t^{(2)}}{V_t}\right) \right] \right\} (1 - E) + E_{2t}} \right]^2 \\
P_{t+1} &= \left[\sqrt{(1 - \mu_1)L_t^{(1)} f\left(\frac{L_t^{(1)}}{V_t}\right) + (1 - \mu_2)L_t^{(2)} f\left(\frac{L_t^{(2)}}{V_t}\right) + E_{3t}} \right]^2 \\
A_{t+1} &= \text{round} [P_t \exp(c_{pa}A_t/V_t)] + \text{round} [(1 - \mu_a)A_t]
\end{aligned} \tag{2}$$

In case the addition of a random term, E_{it} , to the squared deterministic part of one of the first three equations of model (1) results in a negative number then the value is set to zero. The reason why the last equation takes the above form is because the parameters c_{pa} and μ_a , were experimentally manipulated to take values 0.01 and 0.7 respectively. The notation “round[x]” means the closest integer to x. The rounding is because the manipulation was done by adding or removing adults in each census and because insects come only in integer numbers.

Methods

Parameter Estimation

In order to obtain estimates for the parameters of the model, we fitted the stochastic model in the data using the Maximum Likelihood method. Solving the equations of the stochastic model for E_{it} ($i=1, 2, 3$) we get:

$$E_{1t} = \sqrt{L_{t+1}^{(1)}} - \sqrt{bA_t \exp[(-c_{e1}L_t^{(1)} - c_{e2}L_t^{(2)} - c_{ea}A_t) / V_t]}$$

$$E_{2t} = \sqrt{L_{t+1}^{(2)}} - \sqrt{\left\{ (1 - \mu_1) \left[1 - f\left(\frac{L_t^{(1)}}{V_t}\right) \right] + (1 - \mu_2) \left[1 - f\left(\frac{L_t^{(2)}}{V_t}\right) \right] \right\} (1 - E)}$$

$$E_{3t} = \sqrt{P_t} - \sqrt{(1 - \mu_1) f\left(\frac{L_t^{(1)}}{V_t}\right) + (1 - \mu_2) f\left(\frac{L_t^{(2)}}{V_t}\right)}$$

Because of the manipulation of the parameters c_{pa} and μ_a , there were no parameters to estimate for the last equation therefore it was not used in the fitting. We assume that the random vector (E_{1t}, E_{2t}, E_{3t}) has a normal distribution with mean vector of zeros and a variance-covariance matrix Σ with the off diagonal elements equal to zero (i.e. zero covariances). The parameters involved in the first equation appear only in the first equation, therefore the best fit parameters values for $b, c_{e1}, c_{e2}, c_{ea}$ are the values which minimize the sum of squared errors $\sum_{t=1}^n (E_{1t})^2$. But because the parameters μ_1, μ_2, h_1, h_2 appear in both equations 2 and 3, under the assumptions we made for the random vector, it follows from the probability density function of a multivariate normal random vector that the best fit parameter values are those which minimise the sum (see appendix for details), $\sum_{t=1}^n \left[\log(v_2) + \log(v_3) + \frac{(E_{2t})^2}{v_2} + \frac{(E_{3t})^2}{v_3} \right]$, where v_2 and v_3 are the unknown variances of E_2 and E_3 considered as unknown parameters. The two sums were minimized (separately) using the Nelder-Mead simplex algorithm.

Model Evaluation

After the model was fitted to the data, we calculated the generalized R^2 values (as it was done in [21]) for each equation for each replicate, including the replicates not used for fitting. The R^2 values are a measure of how much of the variability of the data is explained by the (deterministic) model. Each equation of the (stochastic) model has the

form $Y_{t+1} = (\sqrt{f(X_t)} + E_t)^2$, where $X_t = (L_t^{(1)}, L_t^{(2)}, P_t, A_t)$ and Y_{t+1} is one of the $L_{t+1}^{(1)}, L_{t+1}^{(2)}, P_{t+1}, A_{t+1}$. If we consider that Y_{t+1} is a real data value at time t+1 and $\sqrt{f(X_t)}$ is the square root of the prediction of the deterministic model for time t+1 using the data values at time t then we have the residuals, $E_t = \sqrt{Y_{t+1}} - \sqrt{f(X_t)}$. The $SSE = \sum_{t=1}^n (E_t)^2$ is the sum of the squared values E_t for a certain equation of the model

for data values drawn from a certain replicate, while the $SST = \sum_{t=1}^n [\sqrt{Y_t} - \text{mean}(\sqrt{Y})]^2$.

Then the R^2 value for the corresponding equation and replicate is calculated as $R^2 = 1 - \frac{SSE}{SST}$. The closer this value is to 1 the more variability is explained by the model. Statistical tests were used to check for normality and autocorrelation of the residuals. The statistical tests done on the residuals were:

1. Shapiro-Wilk test ([26]) on the residuals of each equation for each replicate and for each “Colour” treatment (combining residuals from replicates within a treatment, separately for each equation) to test if the residuals came from a normal distribution.
2. Durbin-Watson test ([27-29]) on the residuals of each equation for each replicate to check for autocorrelation in the residuals.
3. Kolmogorov-Smirnov test for each equation for each pair of replicates to test if the residuals came from the same distribution.

Confidence Intervals

In order to calculate confidence intervals for the parameter estimates, 2000 bootstrapped data sets were created. The bootstrapping was done by resampling the residuals. That is, in order to create a “fake” replicate we start with the initial values $L_0^{(1)}, L_0^{(2)}, P_0, A_0$ of a replicate from the real data (every replicate in the data had the same initial conditions).

Then we randomly choose a triplet (E_{1t}, E_{2t}, E_{3t}) from the residuals obtained from the fitting and we create the values $L_1^{(1)}, L_1^{(2)}, P_1, A_1$ using the stochastic model. In case a sum under a square root was negative the predicted value was set to zero. We repeat the process until the “fake” replicate has as many data as the real one. If the “fake” replicate we wanted to create was a (fake) control replicate the triplet (E_{1t}, E_{2t}, E_{3t}) was chosen randomly from the corresponding residuals of the control replicates, otherwise it was randomly chosen from the rest of the residuals. After doing the above for every replicate we have a complete “fake” data set. After each “fake” data set is created we fit in the model and obtain new estimates for the parameters. After collecting (2000 in our case) sets of parameter estimates we can obtain 95% confidence intervals by calculating the 0.025 and 0.975 quantiles from the estimated set of values for each parameter. The bootstrapping method is a way of trying to estimate what would happen if the experiment was to be repeated many times. The bootstrapped parameter estimates were also used to calculate confidence intervals for the maximum Lyapunov exponents which are discussed in the following paragraph.

Lyapunov Exponents

Starting with an initial condition $X_0 = (L_0^{(1)}, L_0^{(2)}, P_0, A_0)$, we can calculate the set $\{X_0, X_1, \dots, X_n\}$ using the deterministic model. The set of all successive states of the system with X_0 as initial condition is called the (forward) orbit of X_0 . The maximum Lyapunov exponent of the orbit is given by the limit (if the limit exists) $\lim_{n \rightarrow \infty} \frac{1}{n} \ln \|J(X_{n-1})J(X_{n-2}) \dots J(X_0)\|$ where $J(X)$ is the Jacobian matrix calculated at X and $\|\cdot\|$ is any matrix norm. The Jacobian matrix $J(X)$ is a linear approximation of the system around a close “neighbourhood” of X . The Jacobian matrix of the n th iteration of the system with initial condition X_0 , $J^n(X_0)$, maps a sphere centred at X_0 with radius one into an ellipsoid. This means that in general the initial distance of some points sufficiently close to X_0 will be magnified (by the non-linear model) while for other points it will shrink. If the length of the k th longest orthogonal axes of the ellipse

is r_k^n then, the k th Lyapunov exponent of the orbit of X_0 is defined as the limit $\lim_{n \rightarrow \infty} \frac{1}{n} \log r_k^n$. A bounded (not going to infinity) orbit with at least one positive Lyapunov exponent which is not asymptotically periodic and does not have any Lyapunov exponent equal to zero is called a chaotic orbit (see [30] for theory). A chaotic orbit indicates that the system might have a chaotic attractor. An attractor, in simple words, is a set towards which a number of initial points (which in total have positive area, volume etc., depending on the system's dimension) converge. In applied cases, like this, it is not easy to prove mathematically that the system is chaotic. A usual practice is to find under what values for the parameters the maximum Lyapunov exponent is positive and with computer simulations see if there is evidence of a chaotic attractor. The numerical calculation of the maximum Lyapunov exponents has been done by implementing an algorithm in R following the scheme described in the appendix of [21].

Software

All the analysis was conducted using R [41], except from the calculation of the Lyapunov spectrum (all the Lyapunov exponents of an orbit) for which the LET (Lyapunov Exponent Toolbox. Author: Steve Wai Kam SIU) for MATLAB [42] was used.

Model Fitting Results

Parameter Estimation

In table 1 are the parameter estimations and the corresponding 95% confidence intervals acquired from the bootstrapping.

Parameter	ML Estimates	95% C.I.
b	12.08540	(11.91162, 12.62482)
ce1	0.1995520	(0.1946968, 0.2120706)
ce2	0.3611847	(0.3431656, 0.3814984)
cea	0.3056472	(0.2780895, 0.3363196)
μ_1	0.1133886	(0.1024374, 0.1290508)
μ_2	0.1398072	(0.1193096, 0.1586580)
h1	1.5020831	(1.485298, 1.519161)
h2	3.079823	(2.944738, 3.229757)

Table 1: Maximum likelihood estimates and 95% confidence intervals.

The estimates of the variance-covariance matrices Σ_1 and Σ_2 of the random terms in the stochastic model for the control and the rest of the replicates respectively are given below. The values were obtained after the fitting by calculating the variances and covariances between the residuals of the first three equations of model (2).

$$\Sigma_1 = \begin{bmatrix} 0.13245232 & 4 & 0.00655025 & 6 & -0.01814237 \\ 0.00655025 & 6 & 0.03566994 & 3 & -0.01023691 \\ -0.01814236 & 5 & -0.01023690 & 5 & 0.08204503 \end{bmatrix}$$

$$\Sigma_2 = \begin{bmatrix} 0.53082742 & -0.03251455 & 0.02058459 \\ -0.03251455 & 0.25706161 & -0.01329814 \\ 0.02058459 & -0.01329814 & 0.25261823 \end{bmatrix}$$

From the scatter-plot matrix of the bootstrap parameter estimates in figure 2 we can see that there was no substantial correlation among the parameters estimates, indicating that no parameter in the model was unneeded, and from the histograms in the diagonal that the distribution of the estimates was approximately normal.

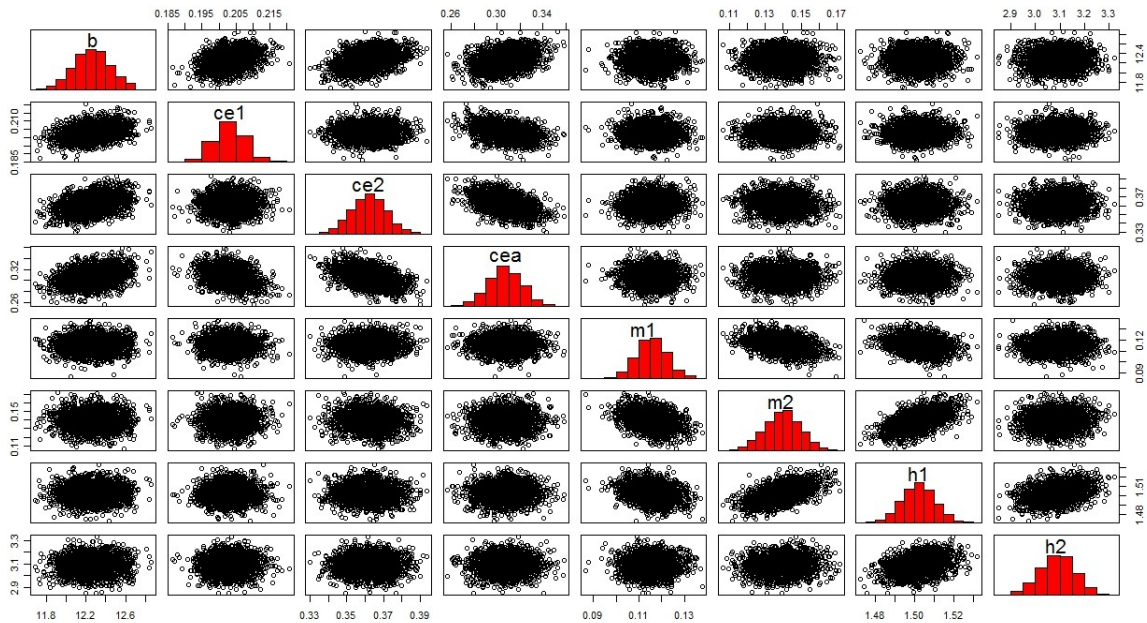


Figure 2: Pair plots of the bootstrap parameter estimates.

Model Evaluation

As mentioned in the methods section, in order to evaluate how well the variability of the data is explained by the model we calculated the generalized R^2 values for each equation (the first three equations of the model) for each of the replicates used for fitting and the ones not used for which R^2 gives a measure of out-of-sample predictive ability of the model. The R^2 values are given in table 2. The AIC (Akaike Information

Criterion) value of the model for the data used for fitting was -31.61591. The AIC value does not provide, by itself, any information on how well the model fits. It has meaning only when compared with the AIC value of a different model. The model with lower AIC value is considered better. A number of slightly different models were fitted (see appendix) but none had better AIC value from the one presented here.

	Equation 1	Equation 2	Equation 3
Replicate 1	0.58522963	0.79979963	-0.09334033
Replicate 2	0.49589773	0.81943425	-0.04237237
Replicate 3	0.4320817	0.5721675	-0.3409283
Replicate 4	0.9854110	0.9773697	0.9885831
Replicate 5	0.9892377	0.9830765	0.9780964
Replicate 6	0.9855375	0.9954118	0.9775155
Replicate 7	0.9848538	0.9862035	0.9909290
Replicate 8	0.9793289	0.9814534	0.9643740
Replicate 9	0.9763612	0.9894264	0.9892925
Replicate 10	0.9932420	0.9936360	0.9645656
Replicate 11	0.9873704	0.9837609	0.9759205
Replicate 12	0.9907734	0.9921892	0.9722996

Table 2: Generalized R^2 values. With red are the replicates that were not used in the fitting.

The R^2 values for equations 1 and 2 for the control replicates are satisfactory. The values for the non-control replicates (4-12), for all three equations, are all very close to 1. This means that the extra variability in the non-control replicates (see figures 5a and 5b) caused by the fluctuations in the habitat volume is explained very well by the model (more than 96% of the variability is explained in every case). The R^2 values for equation 3 for the control replicates (1, 2 and 3) are very low. These values show that equation 3 is performing more or less the same as if we were making predictions using

the mean of the data for the P-stage for each replicate. Does this mean that equation 3 is not good? The average of the absolute values of the differences between the predictions from equation 3 and the real data from all the control replicates (replicates 1, 2, 3) is 3.114443, while the mean the of pupae values in these replicates is 41.79339. Also from the histogram of these differences in figure 3 we can see that equation 3 is indeed doing well in predicting the numbers of pupae.

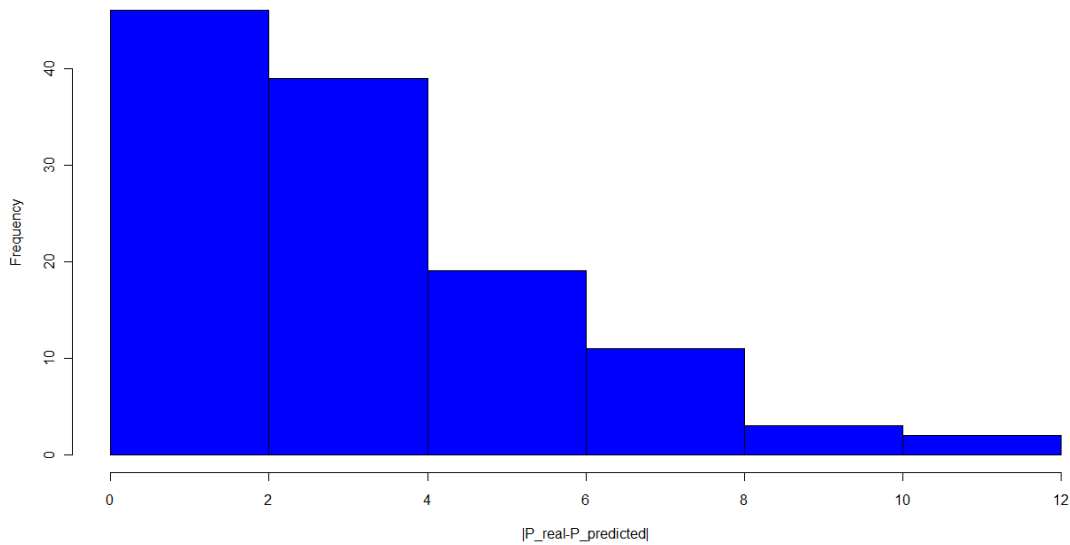


Figure 3: Histogram of the distances between the predicted pupae values and the real data pupae values for replicates 1, 2 and 3.

The reason why the R^2 values for equation 3 for the control replicates 1, 2 and 3 are low is because there is no substantial enough variation from the mean of the pupae values to be explained. In order to give a visual notion of this, figure 4a shows a plot of equation 3 (as a surface) along with the corresponding data values of all the control replicates (1, 2 and 3). In figure 4b the surface is plotted for smaller range of $L^{(1)}$ and $L^{(2)}$ values while in figure 4c instead of the equation surface there is a horizontal plane with the mean of the pupae values as intercept. With green are the points above the surfaces and with red those below (the graphs are presented in such angles so as the data points along with the fitness of the surfaces are as visible as possible). Note that in the data points are also those from control replicate 3 which was not used in the fitting.

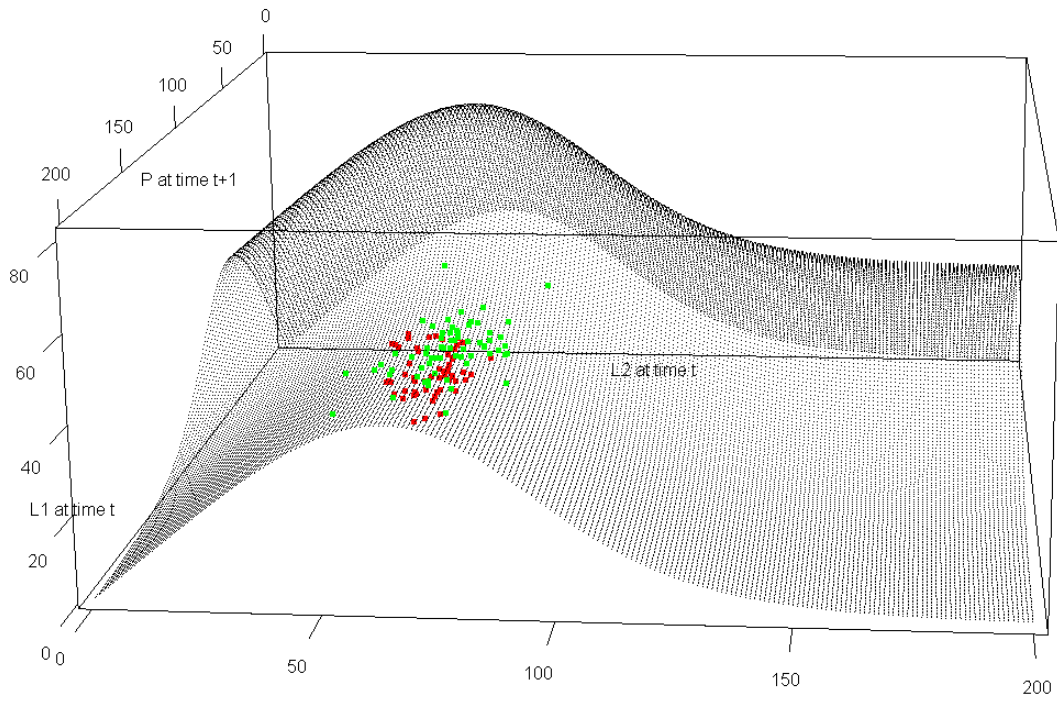


Figure 4a: Equation 3 plotted as a surface along with the corresponding data points from the control replicates 1, 2 and 3. With green are the points above the surface while with red those below.

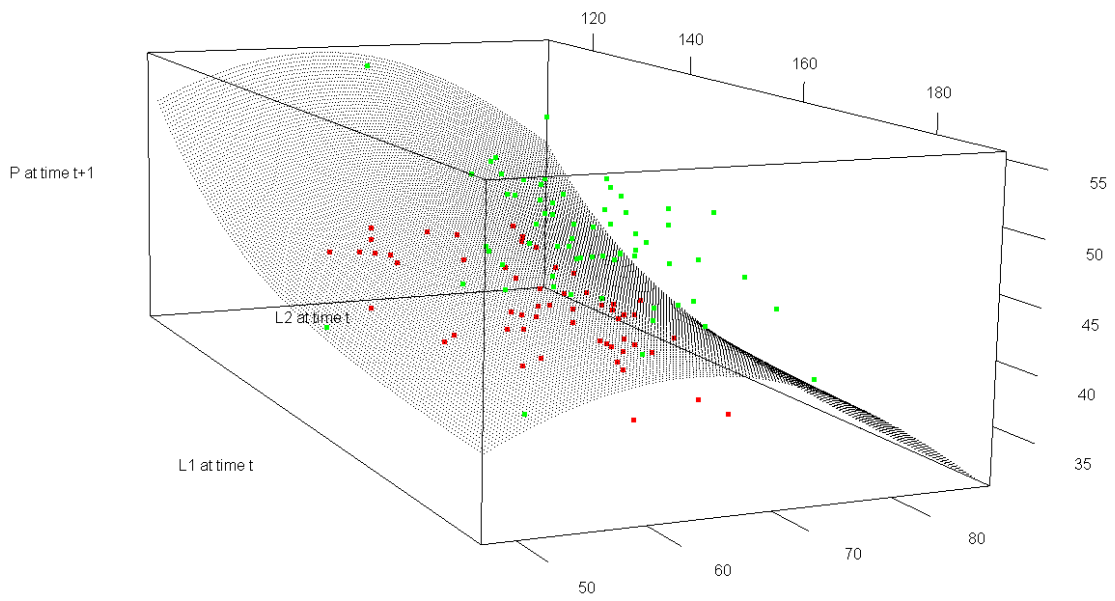


Figure 4b: A closer look on the surface of figure 3a where the data points are concentrated.

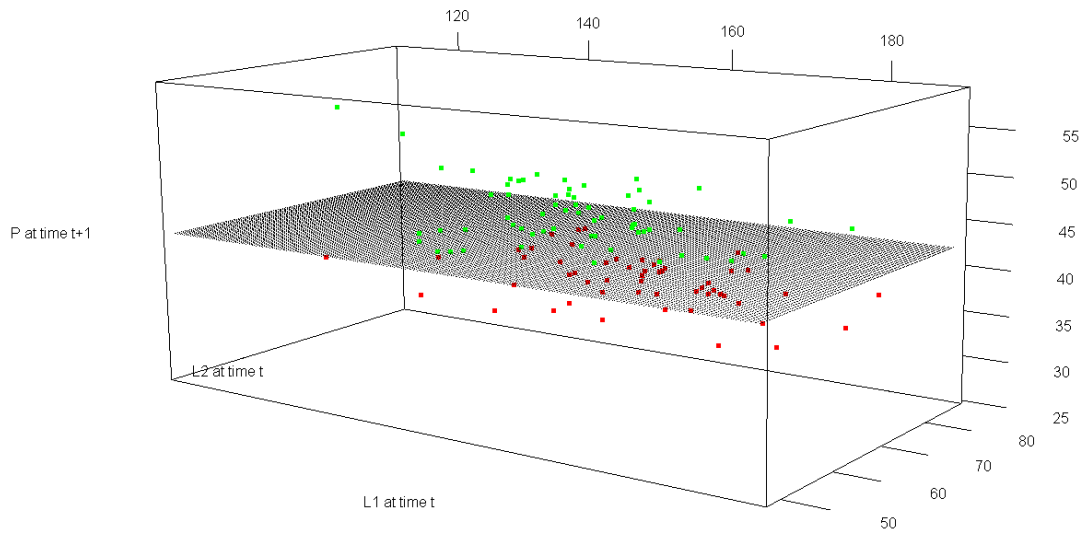


Figure 4c: The plane with intercept the mean of the pupae values in the control replicates 1, 2 and 3 along with the data points from those replicates. With green are the points above the plane while with red those below.

Figure 5a shows the projection of the data points and the plane of figure 4c on the L1 at time t, P at time t+1 plane in order to give a better picture of the small variation of pupae from their mean in the control replicates. For comparison the same was done for the L2 stage (which is predicted by equation 2) in figure 5b.

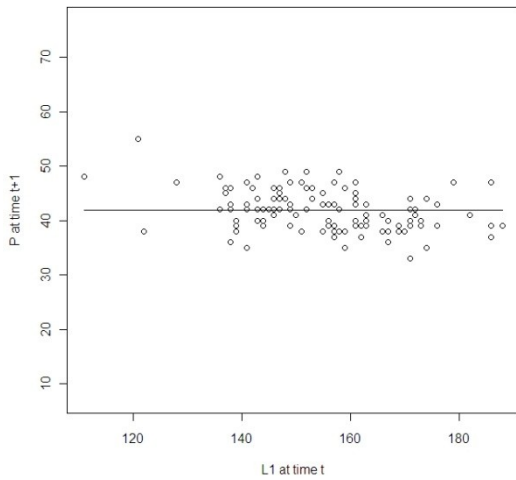


Figure 5a: Small variation from the mean.

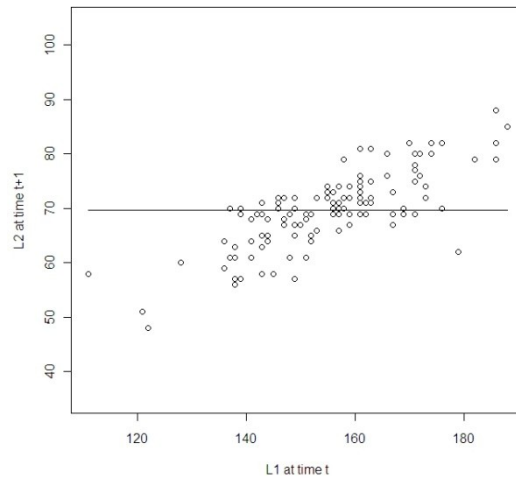


Figure 5b: Larger variation from the mean.

Table 3 shows the SSE and SST values for equations 1, 2 and 3 for the control replicates. Notice that the SST values for equation 3 are always smaller from those of the other equations.

Replicate 1	SSE	SST
Equation 1	7.247521	17.47358
Equation 2	1.804384	9.01289
Equation 3	4.117422	3.76591
Replicate 2	SSE	SST
Equation 1	4.719977	9.363134
Equation 2	1.022360	5.661984

Equation 3	2.693146	2.58367
Replicate 3	SSE	SST
Equation 1	5.851134	10.30278
Equation 2	2.618583	6.120579
Equation 3	3.955057	2.949491

Table 3: SSE and SST values for equations 1, 2 and 3 for the control replicates.

Another way to see if the model is doing well is to look on the time series for the $L^{(1)}$, $L^{(2)}$ larvae stages and for the pupae and the corresponding one step predictions. In figure 6a in blue circles are the time series of the data of replicate 3 for each of the three stages (and volumes) while the red circles are the one step predictions from the deterministic model. Figure 6b shows the same as figure 6a but for replicate 6.

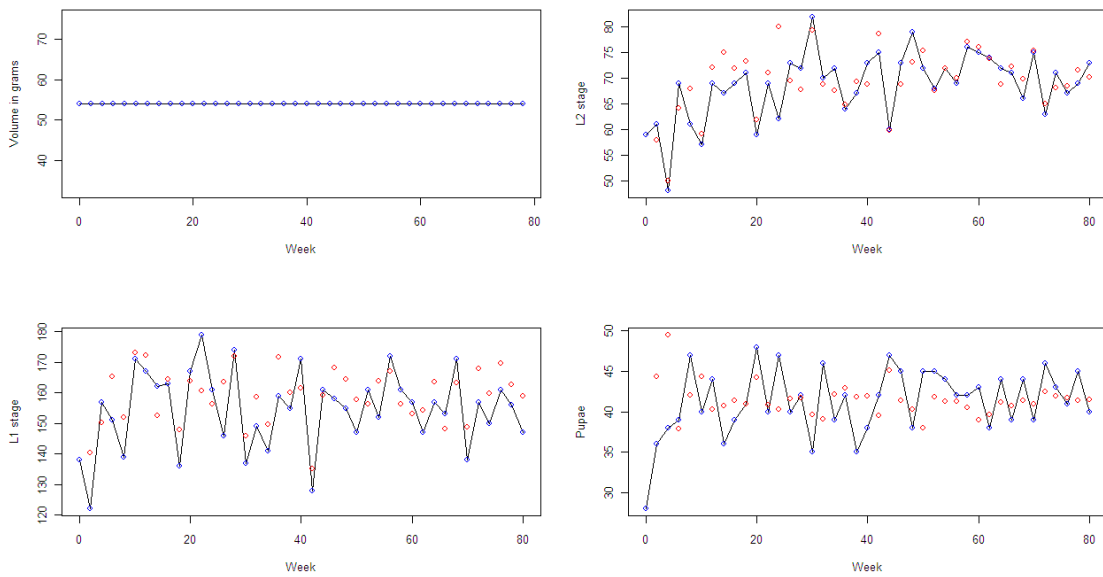


Figure 6a: Times series of replicate 3 and the corresponding one step predictions.

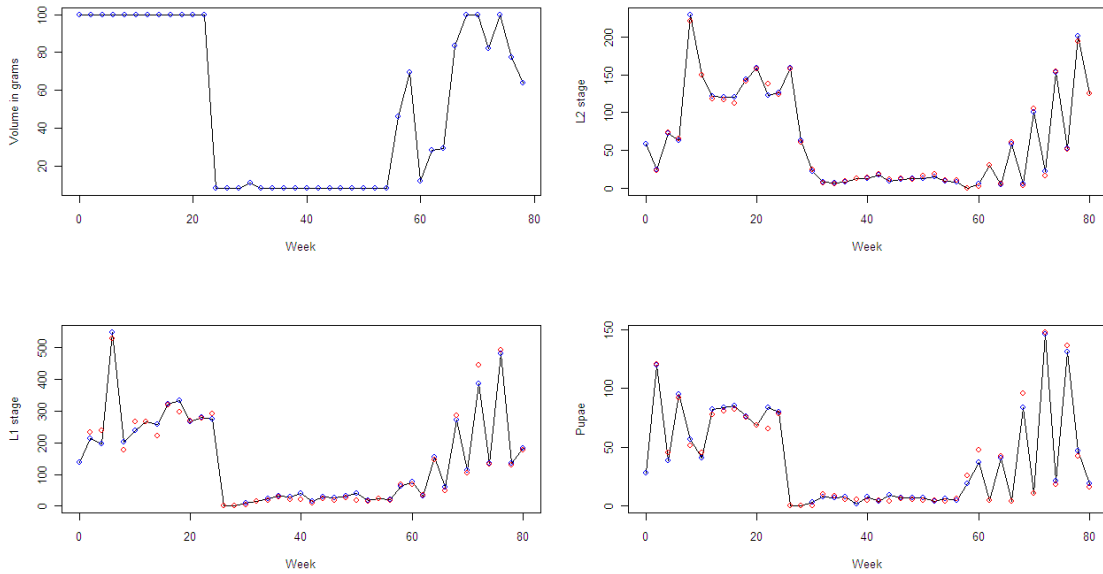


Figure 6b: Time series of replicate 6 and the corresponding one step predictions.

First, remember that replicates 3 and 6 were not used in the fitting. Also notice in figure 6a that for the pupae stage (which had low R^2 values) except from the fact that the errors in predictions are not big, the directions in most of the one step predictions are correct. It is obvious from figure 6b that for the non control replicate 6 the model is doing very well. The two figures of times series are representative of the general “picture” of the times series and the one step predictions for the rest of the replicates (see also appendix). Because of the volume fluctuations in the non control replicates the noise does not have a big impact. On the other hand, in the control replicates because the population is in equilibrium, noise has an effect that is easily visible from the time series.

The analysis of the residuals showed that there was no autocorrelation and that the residuals in each replicate came from the same distribution. There were departures from normality though, for the residuals of equations 2 and 3. Tables with the p-values and the test statistic values from the analysis are given in the appendix.

Chaos and Discrete State Dynamics

Following the footsteps of the work presented in [17] for the dynamics of *T. castaneum* we wanted to see for what parameter manipulations the deterministic model predicts chaotic behaviour. But, as mentioned in [21], it is also important to estimate confidence intervals for the maximum Lyapunov exponents. We will also refer to what is the connection of the continuous state model (populations can take non integer values) with a discrete state version model when the continuous state model predicts chaotic dynamics. We will refer to the corresponding dynamics of the discrete state model as underlying chaos since mathematically a discrete state model cannot be chaotic. In the following, the reader should assume that $E=0.55$, $V_t = 54$, $c_{pa} = 0.01$, $\mu_a = 0.7$ and all the other parameter values were set to the estimated values from the fitting (shown in table 1), otherwise if a parameter varies or has given a different value it will be stated.

Chaotic dynamics

The model has in total 12 (including volume) parameters. Three of them, c_{pa} , μ_a and E were manipulated experimentally. Figure 7 shows the bifurcation diagram of the total population when the parameter for imposed emigration rate of $L^{(2)}$ larvae, E , is set to 0.35 and the adult mortality rate, μ_a , varies from 0 to 1. The bifurcation diagram gives a first notion of what is the dynamical behaviour of a certain orbit, after transients are removed, for different values of the parameter μ_a . The initial conditions used for producing the bifurcation diagram were $(L_0^{(1)}, L_0^{(2)}, P_0, A_0) = (138, 59, 28, 35)$. Vertically separate strands, in the bifurcation diagram, indicate that the orbit ended up in a cycle (periodic behaviour). Values of the parameter μ_a where the total population values seem to fill whole intervals indicate aperiodic orbits. For aperiodic orbits the maximum Lyapunov exponent might be zero indicating that the orbit ends up in an invariant loop, the orbit on an invariant loop though is not chaotic. When the maximum Lyapunov exponent is positive this is an indication that a chaotic attractor might exist. Below the

bifurcation diagram, in figure 8 there is a plot of the maximum Lyapunov exponent values for the different values of μ_a (when $E=0.35$).

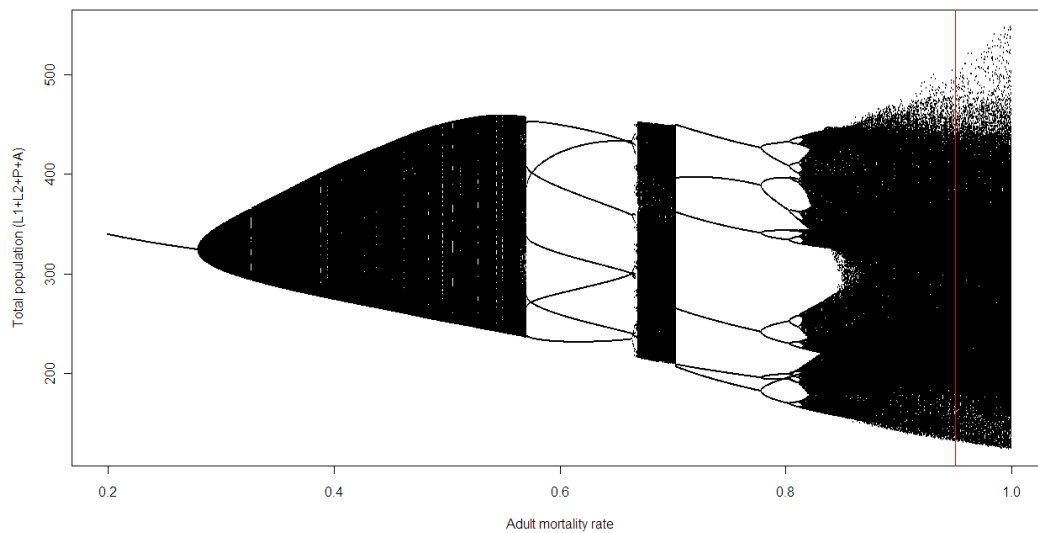


Figure 7: Bifurcation diagram of the total population with μ_a varying ($E=0.35$). The red line indicates where $\mu_a = 0.95$.

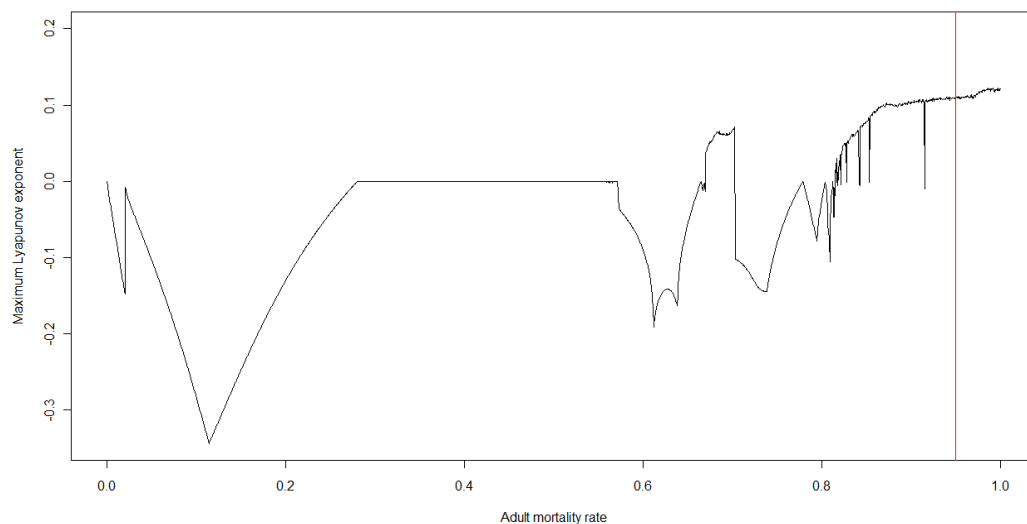


Figure 8: Maximum Lyapunov exponents for varying values of μ_a ($E=0.35$). The red line indicates where $\mu_a = 0.95$.

When $E=0.35$ and $\mu_a = 0.95$ model (1) predicts that the system will have a global (as seen by simulations) chaotic attractor. The maximum Lyapunov exponent is ≈ 0.11 while the corresponding 95% confidence interval is (0.09152199, 0.11486884). Also the simulations, using the 2000 parameters sets obtained from the bootstrapping, showed that the attractor is robust, in the sense that in most of the cases its shape did not affected substantially by the differences in the parameters. Below is a histogram of the 2000 maximum Lyapunov exponents calculated using the 2000 bootstrapped parameter estimate sets.

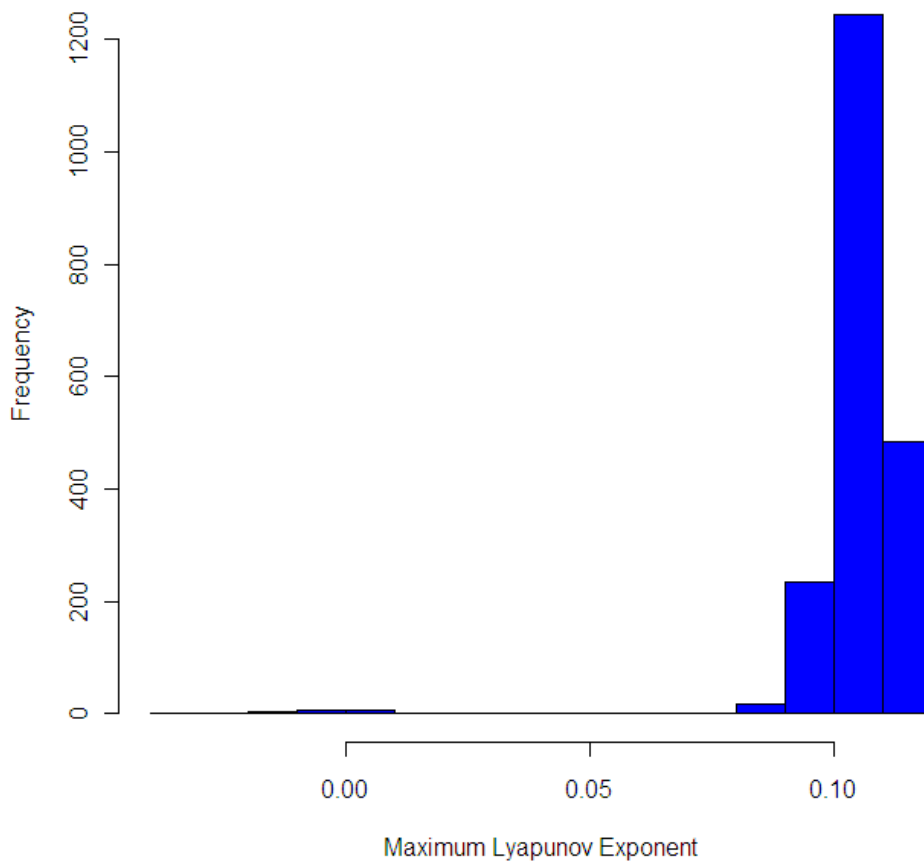


Figure 9: Histogram of the max. Lyapunov exponents calculated from the 2000 bootstrapped parameter estimate sets.

Figure 10 shows a 3D plot of the chaotic attractor. This picture is but a “shadow” of the real attractor since the system is four dimensional and $L^{(1)}$ larvae stage is missing from the phase space.

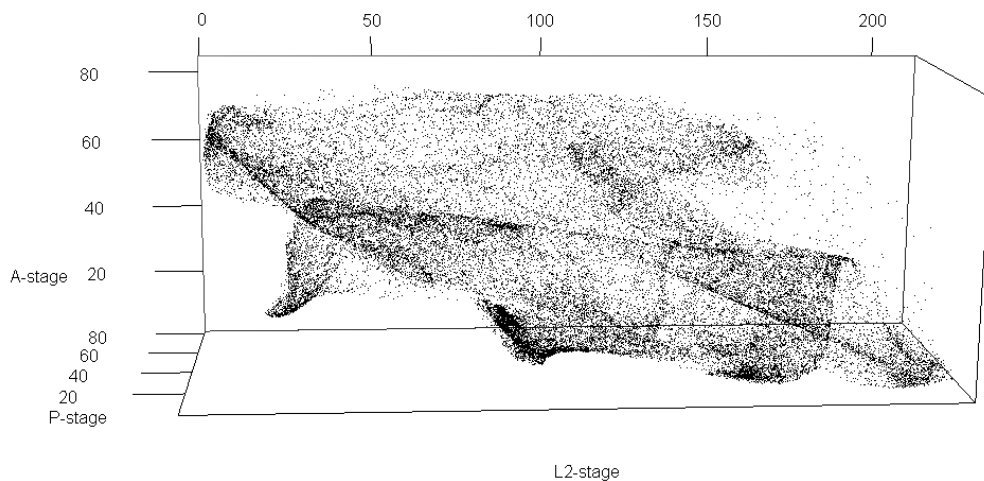


Figure 10: The chaotic attractor of the system when $E=0.35$ and $\mu_a = 0.95$.

The attractor is actually a hyperchaotic attractor [31,32]. Except from the maximum Lyapunov exponent there are two other positive Lyapunov exponents (from the total of four Lyapunov exponents that an orbit has since the system is 4-dimensional). Hyperchaos is the case where at least two Lyapunov exponents are positive (see also section “Lyapunov Dimension” in the appendix).

As mentioned in the introduction, there is more than one mathematical definition of chaos and the common feature shared among them is the sensitivity to initial conditions [8]. Figures 11a, 11b, and 11c, illustrate this feature of the system by depicting how the orbits of a set of initial conditions slightly apart one from another will diverge after a number of time steps using model (1) with $E=0.35$ and $\mu_a = 0.95$.

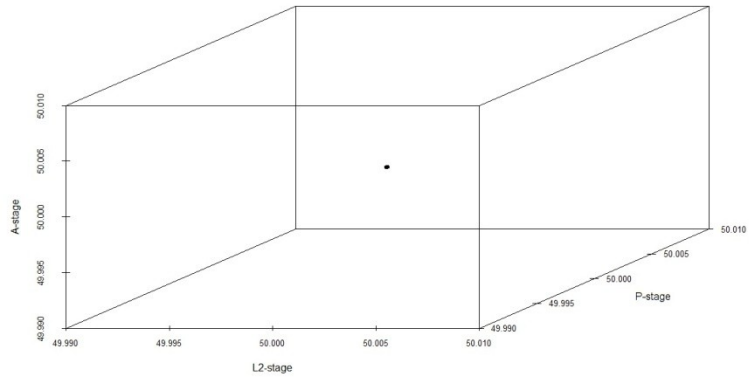


Figure 11a: A sphere of initial conditions with radius 0.0001.

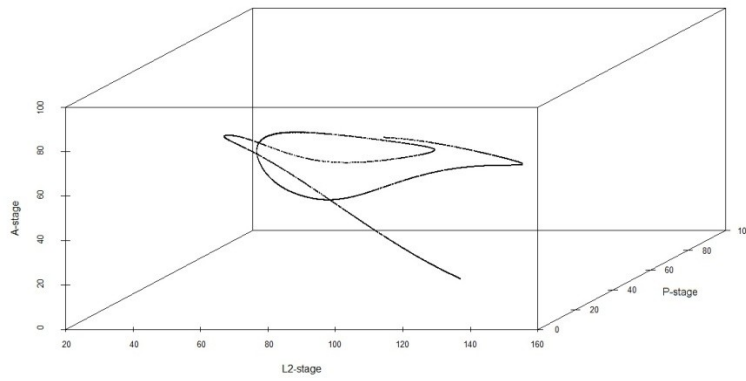


Figure 11b: After 130 iterations.

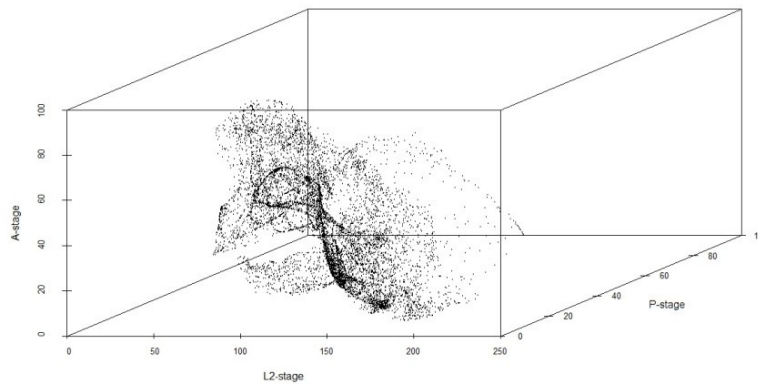


Figure 11c: After 200 iterations.

Discrete State Dynamics and Underlying chaos

Since, in reality, insects come only in integer numbers, one could ask what would happen if we modify model (1) so that the state variables of the system are allowed to take only integer values. Since the orbits of the model are bounded it is easy to see that the integerization of the model would have as a result the existence of only periodic cycles in the dynamic behaviour of the system (see for example [33]). So then the question is: Does the chaotic dynamics predicted by the continuous state model have any real meaning? Is there going to be anything different in the dynamics of the discrete state model for parameter values where the continuous state model behaves chaotically from parameter values where the continuous state model has a periodic cycle? The point made in [17], for the *T. castaneum* model, is that the more the habitat volume increases the more the dynamics of the discrete state model will resemble those of the continuous one. Before this feature is illustrated for the model presented here, below, is the discrete state version of model (1). Note that the convergence of the discrete state attractor to the one of the continuous state model, as the volume increases, is based on simulations and not on a rigorous mathematical proof.

$$\begin{aligned}
L_{t+1}^{(1)} &= \text{round} \left[bA_t \exp \left(\left[-c_{e1}L_t^{(1)} - c_{e2}L_t^{(2)} - c_{ea}A_t \right] / V_t \right) \right] \\
L_{t+1}^{(2)} &= \text{round} \left\{ \text{round} \left((1 - \mu_1)L_t^{(1)} \left[1 - f \left(\frac{L_t^{(1)}}{V_t} \right) \right] + (1 - \mu_2)L_t^{(2)} \left[1 - f \left(\frac{L_t^{(2)}}{V_t} \right) \right] \right) (1 - E) \right\} \\
P_{t+1} &= \text{round} \left((1 - \mu_1)L_t^{(1)} f \left(\frac{L_t^{(1)}}{V_t} \right) + (1 - \mu_2)L_t^{(2)} f \left(\frac{L_t^{(2)}}{V_t} \right) \right) \\
A_{t+1} &= \text{round} \left[P_t \exp \left(-c_{pa}A_t / V_t \right) \right] + \text{round} \left[(1 - \mu_a)A_t \right]
\end{aligned} \tag{3}$$

Figures 12a, 12b, and 12c show the attractor of the system by model (3) when $E=0.35$ and $\mu_a = 0.95$ for different values of (constant throughout time) volume. Note that the graphs below show the periodic attractor of a certain initial condition each time. There are also other periodic attractors, similar to the chaotic attractor from model (1), lying very close to each other. Also, as the volume increases the dynamics of a group of initially close to each other state conditions of the system will “imitate” those in figures 11a, 11b and 11c. Although in the discrete case the minimum difference of two initial conditions is one individual this difference is becoming relatively smaller as the volume increases, either if it is seen as density, $1/V$, or as relative to the total population which is becoming larger as the volume increases.

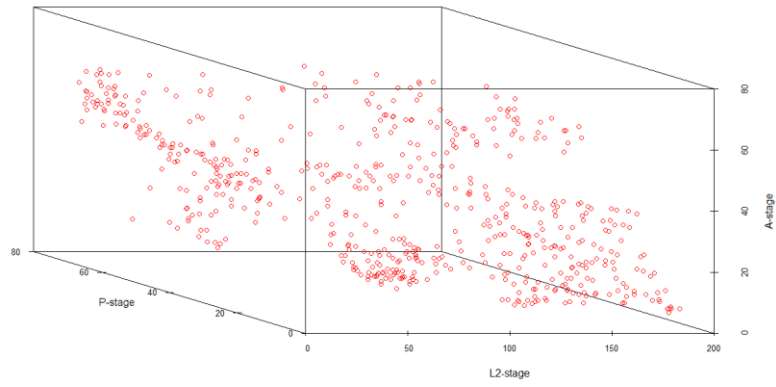


Figure 12a: Attractor by model (3) when volume is set to 50g.

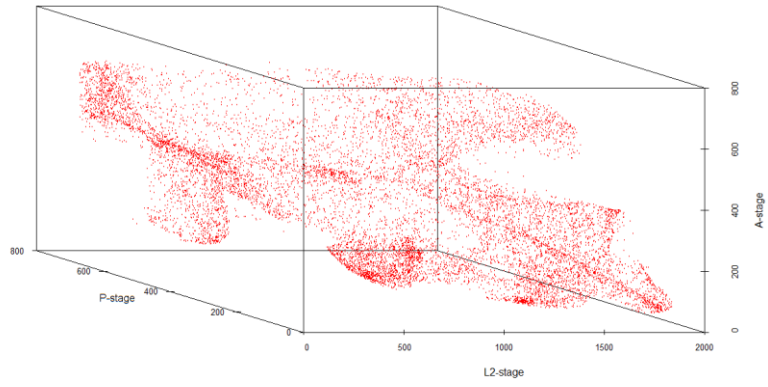


Figure 12b: Attractor by model (3) when volume is set to 500g.

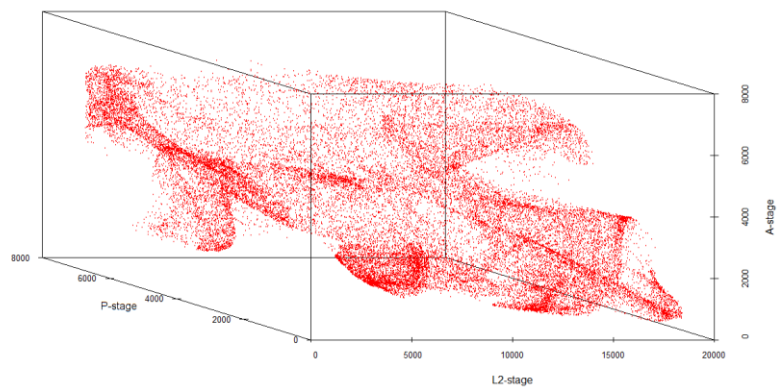


Figure 12c: Attractor by model (3) when volume is set to 5000g.

A Proposed Experimental Scheme

The validation of the model would require the comparison between the predicted behaviour and real data. In the same way used for the *T. castaneum* ([13]), the experimentalist could try to verify the dynamics predicted by the bifurcation diagram in figure 7 by manipulating the adult mortality rate for a number of different values. The interest of this work, though, is mostly on the chaotic and underlying chaotic behaviour predicted by models (1) and (3) respectively. First, below is the stochastic version of model (3).

$$\begin{aligned}
 L_{t+1}^{(1)} &= \text{round} \left[\left(\sqrt{bA_t \exp[-c_{e1}L_t^{(1)} - c_{e2}L_t^{(2)} - c_{ea}A_t] / V_t} + E_{1t} \right)^2 \right] \\
 L_{t+1}^{(2)} &= \text{round} \left(\text{round} \left(\left[\sqrt{(1-\mu_1)L_t^{(1)} \left[1 - f\left(\frac{L_t^{(1)}}{V_t}\right) \right] + (1-\mu_2)L_t^{(2)} \left[1 - f\left(\frac{L_t^{(2)}}{V_t}\right) \right] + E_{2t}} \right]^2 \right) \right) (1-E) \right) \\
 P_{t+1} &= \text{round} \left(\left[\sqrt{(1-\mu_1)L_t^{(1)} f\left(\frac{L_t^{(1)}}{V_t}\right) + (1-\mu_2)f\left(\frac{L_t^{(2)}}{V_t}\right) + E_{3t}} \right]^2 \right) \\
 A_{t+1} &= \text{round} \left[P_t \exp(-c_{pa}A_t / V_t) \right] + \text{round} \left[(1-\mu_a)A_t \right]
 \end{aligned} \tag{4}$$

Based on the facts that as the volume increases the dynamics of model (3) will resemble more the dynamics of model (1), the effect of demographic noise will be smaller, the obtained confidence interval for the maximum Lyapunov exponent when $E=0.35$ and $\mu_a = 0.95$, and the robustness of the attractor, the following experimental scheme is proposed in order to investigate if there would be any (qualitative) evidence of the predicted behaviour in real data.

The basic idea is to collect data, in a relatively small period of time, by culturing *T. freemani* and imposing the manipulations mentioned in the above and after the data is collected to see if the picture we get by plotting the data in the phase space $(L^{(2)}, P, A)$ is similar to the predicted one. There are two things to notice. The first is that because the number of data required is large (relative to the time scale) a number of cultures should be initiated for different initial conditions which by model (3) belong to the “chaotic” attractor. The second is that, in general, because of the presence of noise, in small volumes the deterministic influence in the real data is not going to be clear even if the picture we get matches adequately with the one by model (4). An example of this argument is given in the following.

Figures 13a, 13b, 14a and 14b have been produced using model (4) with the random vector (E_1, E_2, E_3) having a multivariate normal distribution with mean vector of zeros and variance covariance matrix the matrix Σ_1 .

Figures 13a and 13b illustrate the outcome of a simulation of the above experimental scheme for different volumes when $E=0.35$, $\mu_a = 0.6$ where model (1) predicts a stable seven-cycle. In figures 14a and 14b the same is done for $E=0.35$ and $\mu_a = 0.7$ where model (1) predicts a chaotic attractor coexisting with a stable six-cycle. Notice that figures 13a and 14a look similar, but in figures 13b and 14b the difference of the underlying dynamics is made clear. The data in each case came from 20 replicates of 60-week length (if possible it would be better to have longer replicates or more replicates with larger volumes). Figure 14c depicts the chaotic attractor when $E=0.35$ and $\mu_a = 0.7$.

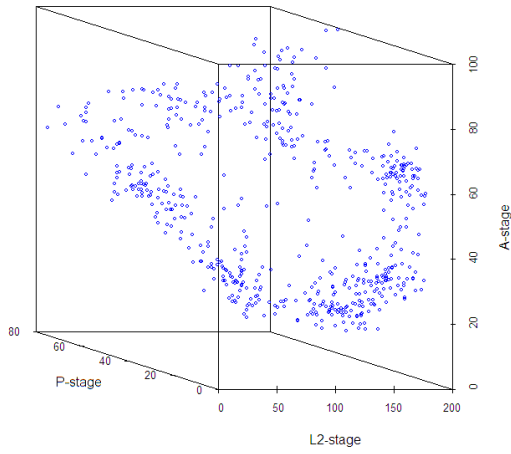


Figure 13a: $E=0.35, \mu_a = 0.6, V=50g$.

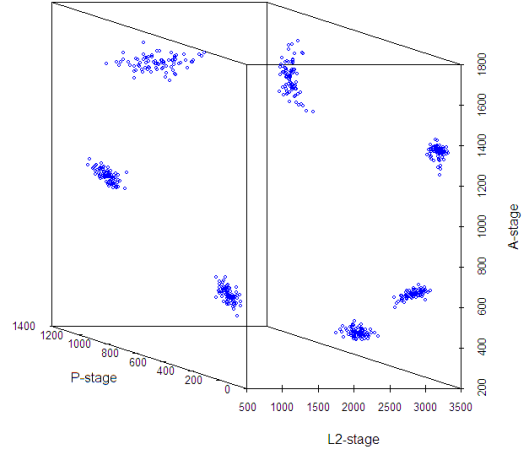


Figure 13b: $E=0.35, \mu_a = 0.6, V=1000g$.

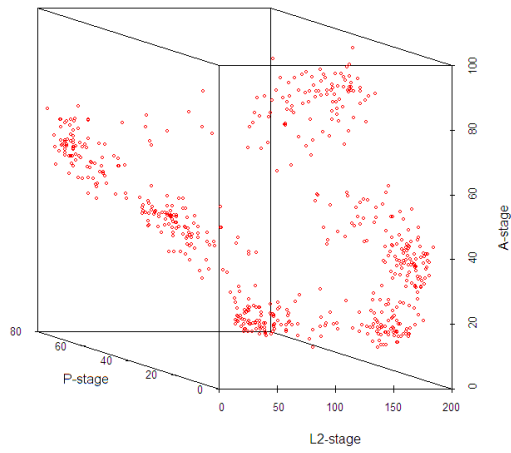


Figure 14a $E=0.35, \mu_a = 0.7, V=50g$.

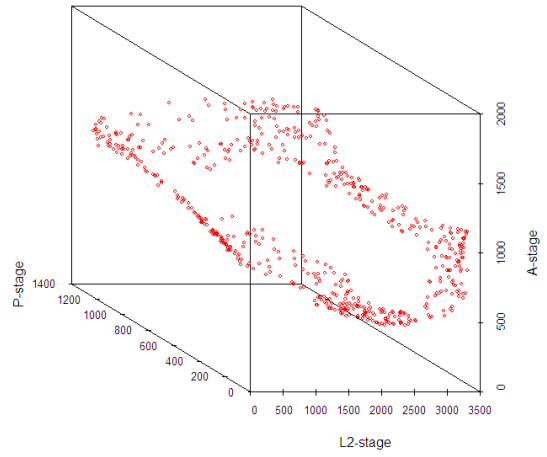


Figure 14b: $E=0.35, \mu_a = 0.7, V=1000g$.

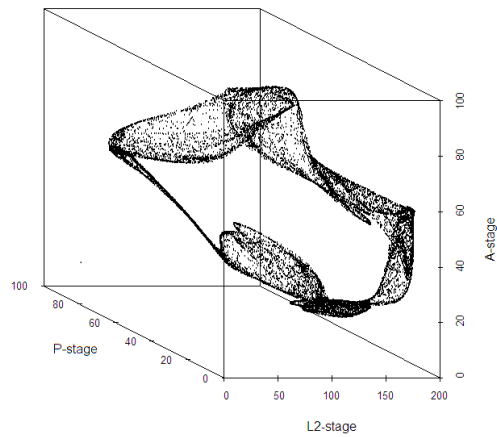


Figure 14c: The chaotic attractor of the system when $E=0.35$ and $\mu_a = 0.7$

In figure 15 the red circles came from model 4 using the same practice, 20 replicates each lasting for 60 weeks and each initiated from a point of the attractor by model (3) with $E=0.35$, $\mu_a = 0.95$ and $V_t = 1000 g$, but the rest of the parameters for each the 20 replicates were randomly chosen from the 2000 bootstrapped parameter estimate sets. The black points are 20000 points simulated with model 3 for the same parameter values.

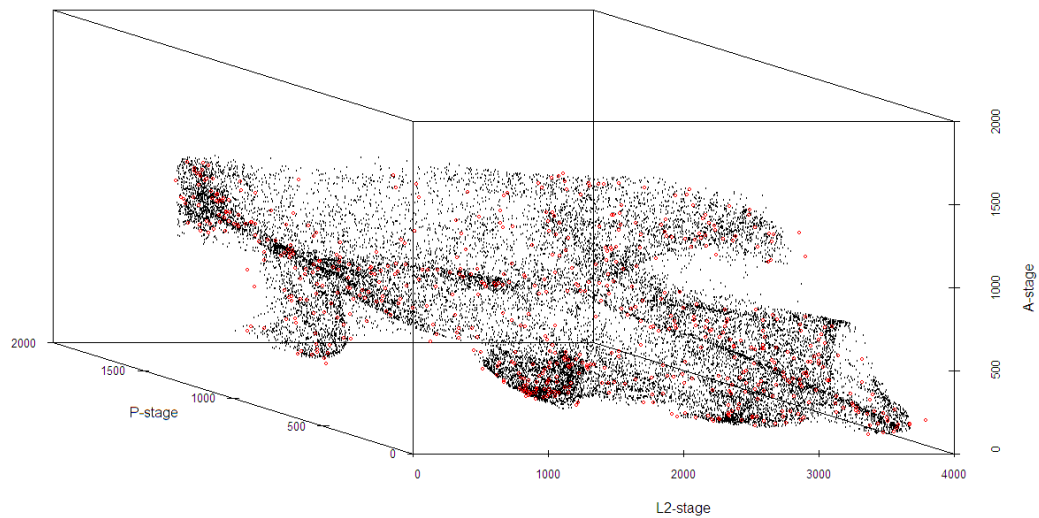


Figure 15: In black: points of the attractor by model 3. The red circles are points from 20 simulations of 30 time steps using model 4 with points of the attractor (black points) as initial conditions ($E=0.35$, $\mu_a = 0.95$ and $V_t = 1000$ g).

An experimental implementation of the above which would give a similar result as the predicted one (red circles in figure 15 “match” with the attractor) would provide good evidence of the chaotic (or underlying chaotic) behaviour of the system (when $E=0.35$, $\mu_a = 0.95$).

One thing to notice is that in large volumes there might be substantial spatial structure that could make the model’s predictions inaccurate. Although after every two weeks the insects would have to be counted so the spatial structure (for example inside the bottles where the insect are cultured) would be destroyed, it might be better to artificially destroy it more frequently.

Discussion

In this work a discrete time model (difference equations) was presented for the population dynamics of the flour beetle *Tribolium freemani*. The model was fitted to experimental data in order to obtain estimations for the parameters of the model. Confidence intervals of the parameters were attained by using a bootstrapping method. The model's fitness was evaluated using as main criterion the generalised R^2 values to see how much of the variation in the data is explained by the model. The results show that the model explains more than 96% of the variation in the non control replicates (where habitat volume was fluctuating). For the control replicates the results were also satisfactory for equations 1 and 2. Only the R^2 values for equation 3 in the control replicates were very low but the reason for that is that there was no substantial variation in the pupae-stage data from their mean which the model could have explained. Most of the one step predictions of equation 3 were very close to the real data.

The above suggest that the model is indeed doing well in describing the dynamics of the population under the experimental conditions. This not only means that the biological mechanisms of cannibalism and inhibition of pupation are driving the intrinsic dynamics of the species but it also reveals the way the inhibition mechanism works (see also appendix). That is, the pupation of ordinary larvae is affected only by crowding of ordinary larvae and respectively the pupation of the delayed larvae only by crowding of the same kind. Also the inhibition function for both larvae types not only has the same form but also the same parameter values.

The model presented here can be used in combination with the model for *T. castaneum* for a theoretical study of the competitive exclusion principle as in [34]. It can also be used for the study of the influence of different kinds of noise on the dynamics as it was done in [35]. As Reuman et al. mention in [35] the influence of noise/stochasticity is of major interest in ecology since it can have a considerable effect on the population dynamics.

The second aim of this work was to identify for what parameter manipulations the model predicts chaotic behaviour in the dynamics of the population. An experimental scheme is suggested on how the predicted "chaotic" dynamics could be observed in real

data, considering the presence of noise. The predicted chaotic dynamics were accompanied by a very high frequency of adequately positive maximum Lyapunov exponents in the 2000 bootstrapped parameter estimates (>99%). A discrete state version of the model (population can take only integer values) and subsequently its stochastic version were considered. A connection was made between the chaotic dynamics of the continuous state model and the discrete state model. We refer to the corresponding dynamics of the discrete state model as underlying chaos as in [17].

If the above were to be validated experimentally, although it would be induced chaos, it would still provide a case of an ecological system where what in first sight might seem as randomness in the dynamics, it can actually be explained by a deterministic model as Robert May's hypothesis suggest. It is possible though, that in natural habitats environmental noise can affect the parameters of the system causing the dynamics to constantly shift from one kind of behaviour (stable) to another (chaotic) and back again. Most importantly, the validation of the above will prove, once again, how successful a mechanistic model can be in explaining population dynamics and demonstrate the value of nonlinear dynamics in ecology.

More general, the search for chaos in the actual dynamics (not induced) of ecological systems does not only have importance under the concept of May's hypothesis but it can also have important applications as in other disciplines. The dynamics of a chaotic system can be controlled and stabilized (see [36-40]) and in fact chaos might be of advantage since, as Ott et al. mention in [36], it might be possible to choose from an infinite number of unstable orbits to stabilize with small parameter perturbations which would not be possible if the system had stable dynamics. Therefore, the identification of chaos in ecological systems yields the possibility for easy control (relatively to case of stable dynamics) of the system, be it for conservation, industrial or medical purposes. The strength of noise though, would play substantial role in the controllability of the system.

Acknowledgements

Many thanks to Dan Reuman, Robert Costantino and Robert Desharnais. Without their guidance and help this project wouldn't exist. Special thanks to Robert Costantino and Robert Desharnais for their valuable conversations and suggestions and to Robert Costantino not only for the data but also for his capability of expressing the ecological system mathematically which provided us with a very accurate model.

References

1. Barrow-Green, J. 1997. *Poincare and the Three Body Problem, History of Mathematics*. American Mathematical Society, Providence, RI.
2. Lorenz, E. N. 1963. Deterministic Nonperiodic Flow. *Journal of the Atmospheric Sciences* **20** : 130-141.
3. Li, T. Y. and York, J. A. 1975. Period three implies chaos. *American Mathematical Monthly* **82** : 985-992.
4. Changpin L. and Guanrong C., 2004. Estimating the Lyapunov exponents of discrete systems. *Chaos* **14** : 343-346.
5. Matsumoto, T., Chua, L.O., and Komuro, M. 1985. The Double Scroll. *IEEE Transactions on Circuits and Systems* **32** : 798-818.
6. Skinner, J. E., Goldberger, A. L., Mayer-Kress, G. and Ideker, R. E. 1990. Chaos in the Heart: Implications for Clinical Cardiology. *Nature Biotechnology* **8** : 1018-1024.
7. Touma, J., Wisdom, J. 1993. The chaotic obliquity of Mars. *Science* **257** : 56-62.
8. Somester, J. 1994. Fractal tracer distributions in complicated surface flows: an application of random maps to fluid dynamics. *Physica D* **76** : 85-98.
9. May, R.M. 1974. Biological populations with nonoverlapping generations: Stable points, stable cycles, and chaos. *Science* **186** : 645-647.
10. May, R.M. 1976. Simple mathematical models with very complicated dynamics. *Nature* **261** : 459-467.
11. Zimmer, C. 1999. Life after chaos. *Science* **284** : 83-86.

12. Ellner, S. and Turchin, P. 1995. Chaos in noisy world: New methods and evidence from time-series analysis. *The American Naturalist* **145** : 343-375.
13. Costantino, R. F., Desharnais, R. A., Cushing, J. M. and Dennis, B. 1997. Chaotic dynamics in an insect population. *Science* **275** : 389-391.
14. Becks, L., Hilker, F. M., Malchow, H., Jurgens, K. And Arndt, H. 2005. Experimental demonstration of chaos in a microbial food web. *Nature* **435** : 1226-1229.
15. Graham, D. W., Knapp, C. W., Van Vleck, E. S., Bloor, K., Lane T. B. and Graham C. E. 2007. Experimental demonstration of chaotic instability in biological nitrification. *ISME Journal* **1** : 385-393
16. Beninca, E., Huisman J., Heerkloss, R., Jöhnk, K.D., Branco, P., Egbert H. Van Nes, Scheffer and M., Ellner, P. 2008. Chaos in a long-term experiment with plankton community. *Nature* **451** : 822-826.
17. Cushing, J. M., Costantino, R. F., Dennis, B., Desharnais, R. A. and Henson, S.M. 2003. *Chaos in ecology: Experimental nonlinear dynamics*. Academic Press, New York.
18. Nichols, J. M. and Nichols, J. D. 2001. Attractor reconstruction for non-linear systems: A methodological note. *Mathematical Biosciences* **121** : 21-32
19. Wolf, A., Swift, J. B. Swinney, H. L. And Vastano J. A. 1985. Determining Lyapunov exponents from a time series. *Physica D* **11** : 285-317.
20. Briggs, K. 1990. An improved method for estimating Liapunov exponents of chaotic time series. *Physics Letters A* **15** : 27-32.

21. Dennis, B., Desharnais, R. A., Cushing, J. M., Henson, S. M. and Costantino, R. F. 2001. Estimating chaos and complex dynamics in an insect population. *Ecological Monographs* **71** : 277-303.
22. Cushing, J. M., Henson, S. M., Desharnais, R. A., Dennis, B., Costantino R. F., King, A. 2001. A chaotic attractor in ecology. *Chaos, Solitons and Fractals* **12** : 219-234.
23. Nakakita, H. 1982. Effect of larval density of pupation of *Tribolium freemani* Hinton (Coleoptera: Tenebrionidae) *Applied Entomology and Zoology* **17** : 269-276.
24. Kotaki, T. Nakakita, H. and Kuwahara, M. 1993. Crowding inhibits pupation in *Tribolium freemani* Hinton (Coleoptera: Tenebrionidae): Effects of isolation and juvenile hormone analogues on development and pupation. *Applied Entomology and Zoology* **28** : 43-52.
25. Kotaki, T. and Fufii, H. 1995. Crowding inhibits pupation in *Tribolium freemani*: contact chemical and mechanical stimuli are involved. *Entomologia Experimentalis et Applicata* **74** : 145-149.
26. Shapiro, S. S. and Wilk, M. B. 1965. An analysis of variance test for normality (complete samples). *Biometrika* **52** : 591-611.
27. Durbin, J. and Watson, G. S. 1950. Testing for serial correlation in least squares regression: I. *Biometrika* **37** : 409-428.
28. Durbin, J. and Watson, G. S. 1951. Testing for serial correlation in least squares regression: II. *Biometrika* **38** : 159-178.
29. Durbin, J. and Watson, G. S. 1971. Testing for serial correlation in least squares regression: III. *Biometrika* **58** : 1-19

30. Alligood, K. T., Sauer, T. D. and Yorke, J. A. 1997. *Chaos: An introduction to dynamical systems*. Springer-Verlag, New York.
31. Kapitaniak, T., Thylwe, K. E., Cohen, I., and Wojewoda, J. 1995. Chaos-hyperchaos transition. *Chaos, Solitons and fractals* **5** : 2003-2011.
32. Thamilmaran, K., Lakshmanan, M., and Venkatesan, A. 2004. Hyperchaos in a modified canonical Chua's circuit. *International Journal of Bifurcation and Chaos* **14** : 221-243.
33. King, A. A., Costantino, R. F., Cushing, J. M., Henson, S. M., Desharnais, R. A. and Dennis, B. 2004. Anatomy of a chaotic attractor. *PNAS* **101** : 408-413.
34. Edmunds, J, Cushing, J. M., Costantino R. F., Henson, S. M., Dennis, B. and Desharnais, R. A. 2003. Park's *Tribolium* competition experiments: a non-equilibrium species coexistence hypothesis. *Journal of Animal Ecology* **72** : 703-712.
35. Reuman, D. C., Desharnais, R. A., Costantino R. F., Ahmad, O. S., and Cohen J. E. 2006. Power spectra reveal the influence of stochasticity on nonlinear population dynamics. *PNAS* **103** : 18860-18865.
36. Ott, E., Grebogi, C. and Yorke, J.A. 1990. Controlling Chaos. *Physical Review Letters* **64** : 1196-1199.
37. Güémez, J., Matías, M. A. 1993. Control of chaos in unidimensional maps. *Physics Letters A* **181** : 29-32.
38. Codreanu, S., Danca, M. 1997. Suppression of chaos in a one-dimensional mapping. *Journal of Biological Physics* **23** : 1-9.

39. Parthasarathy, S., Sinha, S. 1995. Controlling chaos in unidimensional maps using constant feedback. *Physical Review E* **51** : 6239-6242.
40. Wieland, C. 2002. Controlling chaos in higher dimensional maps with constant feedback: An analytical approach. *Physical Review* **66** : 1-8.
41. R Development Core Team (2010). R: A language and environment for statistical computing. R Foundation for Statistical Computing, Vienna, Austria. ISBN 3-900051-07-0, URL <http://www.R-project.org>.
42. The MathWorks Inc. 2010. MATLAB R2010b, Natick, Massachusetts.

Appendix

Parameter Estimation

The probability density function of a normally distributed random vector $E = (E_1, E_2, E_3)$ with mean vector μ and variance-covariance matrix Σ (Σ must be a

positive-definite matrix) is, $f(E) = (2\pi)^{-k/2} |\Sigma|^{-1/2} \exp\left[-\frac{1}{2}(E - \mu)^T \Sigma^{-1}(E - \mu)\right]$.

In our case $k=3$. We assumed that $\mu = [0 \ 0 \ 0]$ and $\Sigma = \begin{bmatrix} v_1 & 0 & 0 \\ 0 & v_2 & 0 \\ 0 & 0 & v_3 \end{bmatrix}$.

Then we

have, $\log [f(E)] = \log [(2\pi)^{-3/2}] - \frac{1}{2} \left(\log(v_1) + \log(v_2) + \log(v_3) + \frac{E_1^2}{v_1} + \frac{E_2^2}{v_2} + \frac{E_3^2}{v_3} \right)$.

Recall that from the statistical model (2) we have,

$$E_{1t} = \sqrt{L_{t+1}^{(1)}} - \sqrt{bA_t \exp[(-c_{e1}L_t^{(1)} - c_{e2}L_t^{(2)} - c_{ea}A_t) / V_t]}$$

$$E_{2t} = \sqrt{L_{t+1}^{(2)}} - \sqrt{\left\{ (1 - \mu_1) \left[1 - f\left(\frac{L_t^{(1)}}{V_t}\right) \right] + (1 - \mu_2) \left[1 - f\left(\frac{L_t^{(2)}}{V_t}\right) \right] \right\} (1 - E)}$$

$$E_{3t} = \sqrt{P_t} - \sqrt{(1 - \mu_1) f\left(\frac{L_t^{(1)}}{V_t}\right) + (1 - \mu_2) f\left(\frac{L_t^{(2)}}{V_t}\right)}$$

In order to find the maximum likelihood parameter values we want to find those values

which maximize the sum $\sum_{t=1}^{320} \log [f(E_t)]$.

That is, to minimize $\sum_{t=1}^{320} \left(\log(v_1) + \log(v_2) + \log(v_3) + \frac{E_{1t}^2}{v_1} + \frac{E_{2t}^2}{v_2} + \frac{E_{3t}^2}{v_3} \right)$. But since the

parameters $b, c_{e1}, c_{e2}, c_{ea}$ appear only in the terms E_{1t} we can find their best fit values by

minimizing $\sum_{t=1}^{320} E_{1t}^2$ regardless of the variance v_1 . But because the parameters

μ_1, μ_2, h_1, h_2 appear in both E_{2t} and E_{3t} their variances must be taken into account and

that is why we have to minimize $\sum_{t=1}^{320} \left(\log(v_2) + \log(v_3) + \frac{E_{2t}^2}{v_2} + \frac{E_{3t}^2}{v_3} \right)$.

The Inhibition Function

Plots of the inhibition function are shown below in figures 14 and 15 in order to demonstrate the difference when varying the h_1 and h_2 parameters of the function.

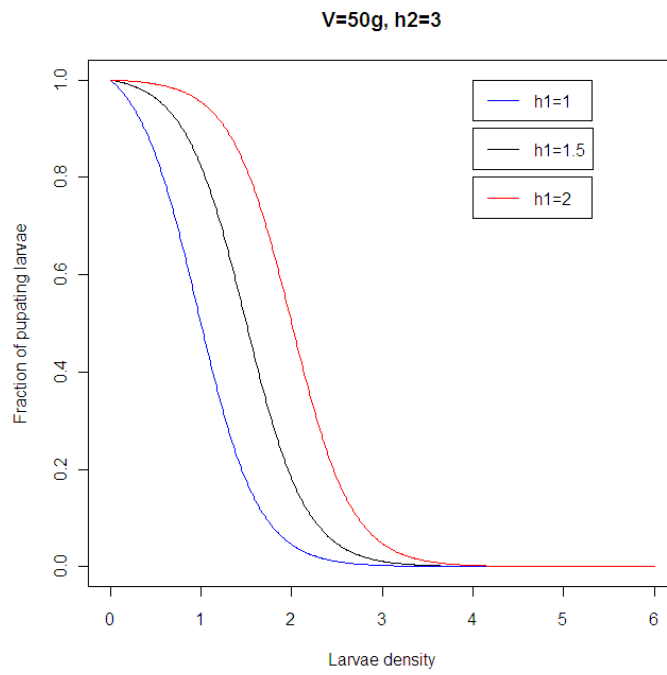


Figure 16a: Plots of the inhibition function for different values of the h_1 parameter.

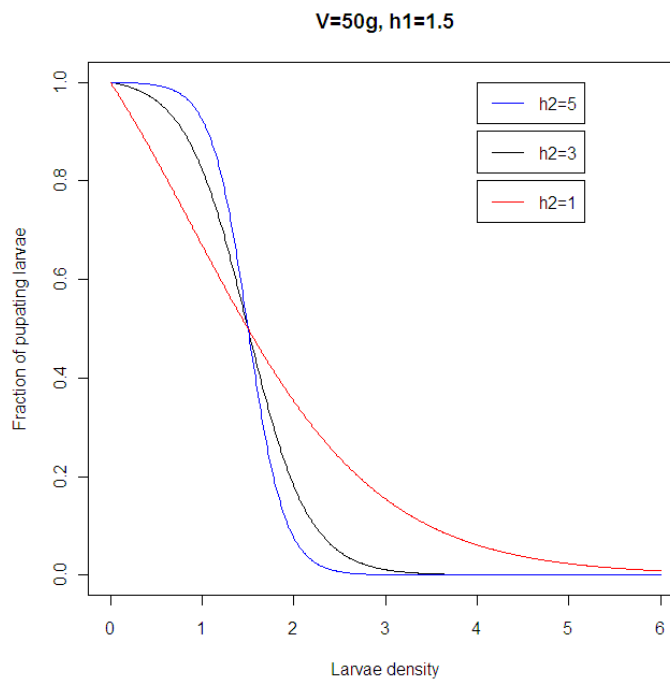


Figure 16b: Plots of the inhibition function for different values of the h_2 parameter.

Results from Statistical Tests on the Residuals

	Residuals of eq. 1	Residuals of eq. 2	Residuals of eq. 3
Replicate 1	0.15098286	0.7060138	0.9697744
Replicate 2	0.15559597	0.1698264	0.5815052
Replicate 4	0.05598482	3.052409e-03	0.01018813
Replicate 5	0.65401285	4.750114e-07	0.01709180
Replicate 7	0.58829388	0.04165070	7.645289e-06
Replicate 8	0.95249445	0.01427521	1.932918e-05
Replicate 10	0.01666762	0.1370599	2.713523e-09
Replicate 11	0.32269019	7.730995e-04	3.148524e-04

Table 3: P-values from the Shapiro-Wilk test for each replicate indicate there are some departures from normality.

	Residuals of eq. 1	Residuals of eq. 2	Residuals of eq. 3
Colour 1	0.04891516	0.2485079	0.5618178
Colour 2	0.23820719	6.560779e-07	1.287303e-03
Colour 3	0.70931294	1.268939e-03	4.152999e-09
Colour 4	0.01804639	2.455742e-05	1.429843e-11

Table 4: P-values from the Shapiro-Wilk test on each colour. More departures from normality. Colour 1 means the control replicates 1-3.

	Residuals of eq. 1	Residuals of eq. 2	Residuals of eq. 3
Replicate 1	1.621840	2.123172	1.549604
Replicate 2	1.837808	2.177252	1.905008
Replicate 4	1.740294	2.066694	1.737756
Replicate 5	1.306382	2.049121	1.947965
Replicate 7	2.006876	1.678927	1.605171

Replicate 8	1.385906	2.176279	1.916320
Replicate 10	2.302899	1.555693	1.783835
Replicate 11	1.594676	2.158711	2.084978

Table 5: Test statistic values from the Durbin-Watson test. The values indicate no autocorrelation problem in the residuals.

	Replicates 1-2	Replicates 1-4	Replicates 1-5	Replicates 1-7
Equation 1	0.09707484	0.0143015480	6.576891e-05	0.014301548
Equation 2	0.91880522	0.5786001417	4.045874e-01	0.578600142
Equation 3	0.16497270	0.0005039436	1.649727e-01	0.001270814
	Replicates 1-8	Replicates 1-10	Replicates 1-11	Replicates 2-4
Equation 1	0.003018184	0.01430155	0.1649726995	0.05414108
Equation 2	0.265687140	0.26568714	0.0067607323	0.09707484
Equation 3	0.014301548	0.01489316	0.0005039436	0.09707484
	Replicates 2-5	Replicates 2-7	Replicates 2-8	Replicates 2-10
Equation 1	0.0005039436	0.05414108	0.02860307	0.26568714
Equation 2	0.0970748438	0.16497270	0.05414108	0.09707484
Equation 3	0.4045874057	0.26568714	0.76593145	0.75909784
	Replicates 2-11	Replicates 4-5	Replicates 4-7	Replicates 4-8
Equation 1	0.1649726995	0.02860307	0.5786001	0.40458741
Equation 2	0.0005039436	0.40458741	0.9999246	0.99992461
Equation 3	0.0970748438	0.09707484	0.9188052	0.01430155
	Replicates 4-10	Replicates 4-11	Replicates 5-7	Replicates 5-8
Equation 1	0.7659315	0.4045874	0.05414108	0.1649727
Equation 2	0.7659315	0.2656871	0.40458741	0.4045874
Equation 3	0.4004737	0.9188052	0.16407920	0.4045874

	Replicates 5-10	Replicates 5-11	Replicates 7-8	Replicates 7-10
Equation 1	0.02860307	0.001270814	0.99001933	0.4045874
Equation 2	0.76593145	0.054141077	0.99001933	0.7659315
Equation 3	0.75909784	0.097104524	0.09707484	0.9134755
	Replicates 7-11	Replicates 8-10	Replicates 8-11	Replicates 10-11
Equation 1	0.2656871	0.5786001	0.09707484	0.05464633
Equation 2	0.2656871	0.9188052	0.16497270	0.40047367
Equation 3	0.5786001	0.4004737	0.16497270	0.75909784

Table 6: P-values from Kolmogorov-Smirnov test for each pair of replicates. A few of these are below 0.01, but generally it seems like a reasonable if not entirely perfect assumption to say the residuals were distributed in the same way across replicates.

Time Series and Corresponding One-Step Predictions

Below are time series plots along with the one step predictions of model (1), as those in figures 6a and 6b, for replicates 1, 4, 9 and 12. Again, remember that replicates 9 and 12 were not used in the fitting.

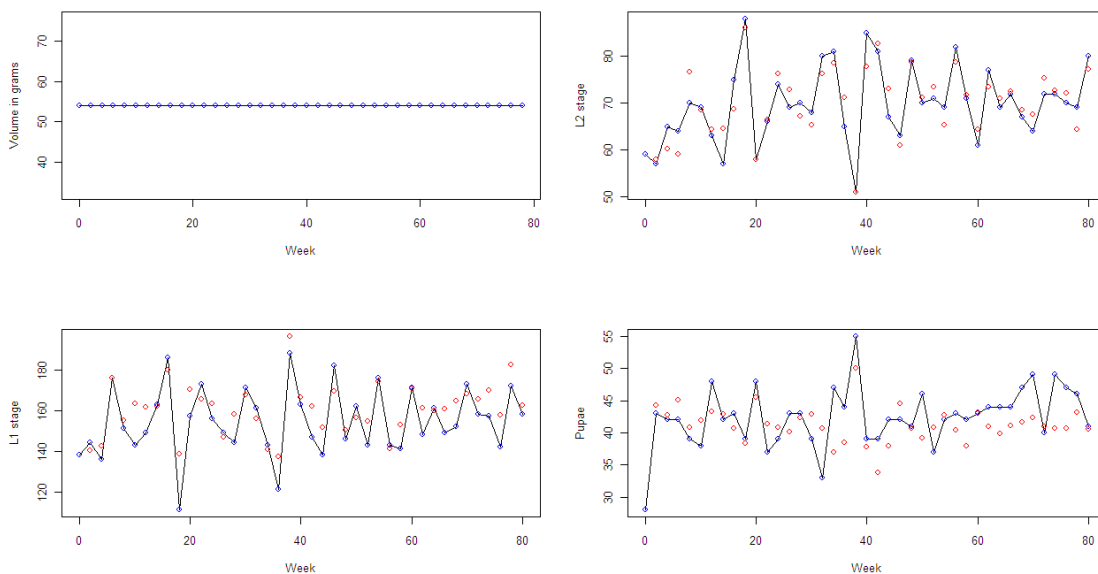


Figure 17a: Times series of replicate 1 and the corresponding one step predictions.

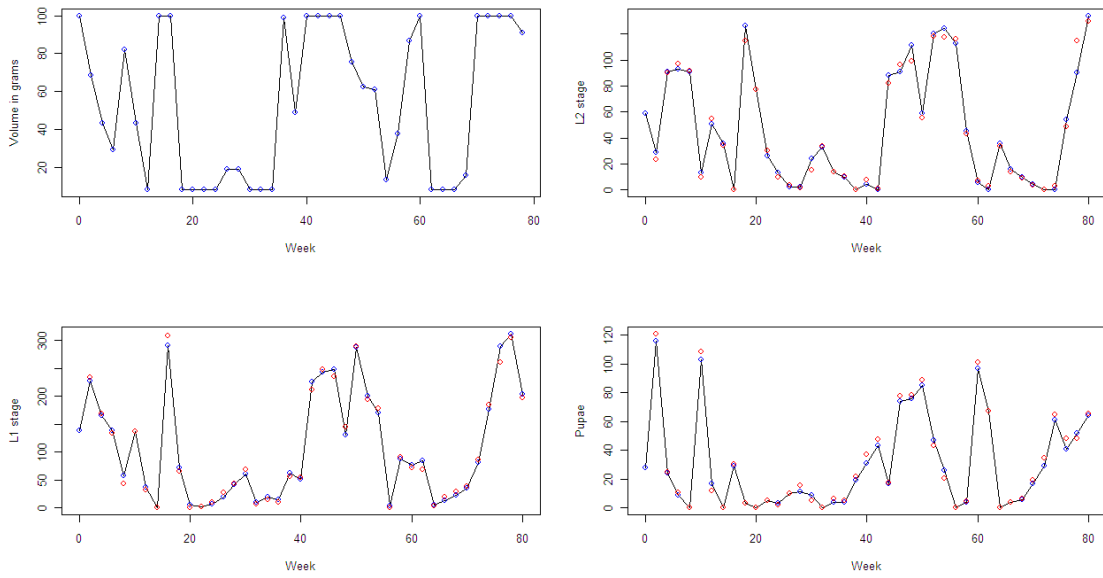


Figure 17b: Times series of replicate 4 and the corresponding one step predictions.

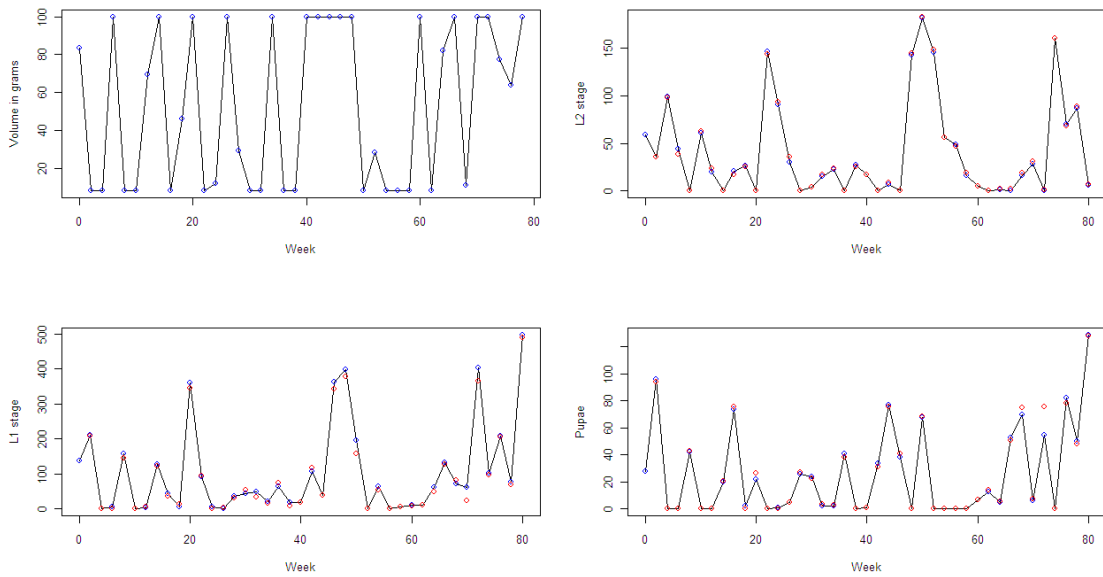


Figure 17c: Times series of replicate 9 and the corresponding one step predictions.

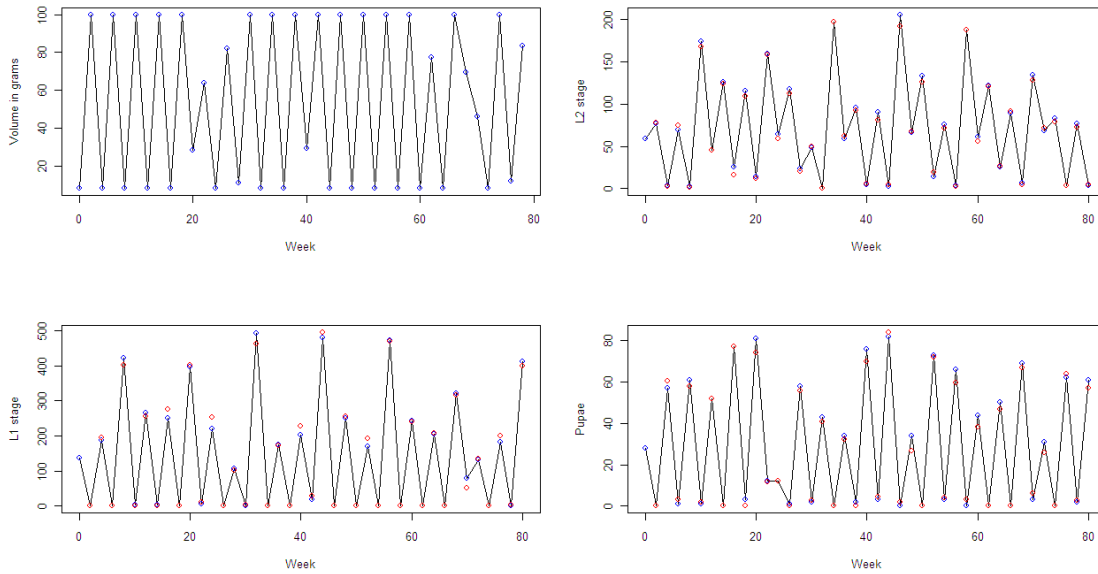


Figure 17d: Times series of replicate 12 and the corresponding one step predictions.

Other Model Trials

As mentioned in the main text, different variants of the model were also fitted but none was better. In the table below are three of them, each one use the same inhibition function as the model presented but in a different way (Only the equations differing from the presented model are shown). Next to each model in the table the corresponding AIC values are shown. In the last model f_1 and f_2 have again the same form of the inhibition function but the corresponding h_1 and h_2 parameters are allowed to take different values for each function (i.e. there are two more parameters h_3 and h_4). The fact that the AIC value for the last model in the table is close to the model presented in the main text indicates that the addition of the two new parameters is not needed. The other model trials included models with different formulas for the inhibition function.

Model	AIC Value
$L_{t+1}^{(2)} = \left[(1 - \mu_1)L_t^{(1)} + (1 - \mu_2)L_t^{(2)} \right] \left[1 - f \left(\frac{L_t^{(1)} + L_t^{(2)}}{V} \right) \right] (1 - E)$ $P_{t+1} = \left[(1 - \mu_1)L_t^{(1)} + (1 - \mu_2)L_t^{(2)} \right] f \left(\frac{L_t^{(1)} + L_t^{(2)}}{V} \right)$ <p>(Both types of larvae affect the pupation of both larvae types.)</p>	480.27
$L_{t+1}^{(2)} = \left\{ (1 - \mu_1)L_t^{(1)} \left[1 - f \left(\frac{L_t^{(1)} + L_t^{(2)}}{V} \right) \right] + (1 - \mu_2)L_t^{(2)} \left[1 - f_2 \left(\frac{L_t^{(2)}}{V} \right) \right] \right\} (1 - E)$ $P_{t+1} = (1 - \mu_1)L_t^{(1)} f \left(\frac{L_t^{(1)} + L_t^{(2)}}{V} \right) + (1 - \mu_2)L_t^{(2)} f \left(\frac{L_t^{(2)}}{V} \right)$ <p>(Both types of larvae affect the pupation of the L1-stage larvae but L2-stage is affected only by the same type of larvae.)</p>	123.84
$L_{t+1}^{(2)} = \left\{ (1 - \mu_1)L_t^{(1)} \left[1 - f_1 \left(\frac{L_t^{(1)}}{V} \right) \right] + (1 - \mu_2)L_t^{(2)} \left[1 - f_2 \left(\frac{L_t^{(2)}}{V} \right) \right] \right\} (1 - E)$ $P_{t+1} = (1 - \mu_1)L_t^{(1)} f_1 \left(\frac{L_t^{(1)}}{V} \right) + (1 - \mu_2)L_t^{(2)} f_2 \left(\frac{L_t^{(2)}}{V} \right)$	-30.44

Table 1 : Different model trials, considering different ways of how the inhibition mechanism might work.

Lyapunov Dimension

(The following definition is taken from [30], where the reader can also find an explanation of the Lyapunov dimension p. 203-207)

Let f be a map on \mathbb{R}^m . Consider an orbit with Lyapunov exponents $h_1 \geq \dots \geq h_m$ and p

denote the largest integer such that $\sum_{i=1}^p h_i \geq 0$. Then the Lyapunov dimension, D_L , of the

orbit is defined as $D_L = p + \frac{1}{|h_{p+1}|} \sum_{i=1}^p h_i$, if $p < m$. If no such p exists then $D_L = 0$ and

if $p=m$ then $D_L = m$.

Because the algorithm implemented for this project (following the instructions in the appendix of [21]) was for the calculation of only the maximum Lyapunov exponent and as seen from the above definition in order to calculate the Lyapunov dimension all the Lyapunov exponents of the orbit are needed (and because of lack of time) the LET (Lyapunov Exponent Toolbox. Author: Steve Wai Kam SIU) toolbox for matlab was used.

The values of the Lyapunov exponents calculated by LET were $h_1 = 0.13007$, $h_2 = 0.066165$, $h_3 = 0.030257$ and $h_4 = -0.68581$.

By the above definition the Lyapunov dimension of the attractor with $E=0.35$, $\mu_a = 0.95$ is **3.3303**.

(The maximum Lyapunov exponent by LET was higher by ≈ 0.02 from the value by the algorithm written for this project)

Also, an attractor with at least two positive Lyapunov exponents (in this case there were three) is called **hyperchaotic**.